Formation Control With Time-Varying Formations, Bounded Controls, and Local Collision Avoidance

Zachary S. Lippay and Jesse B. Hoagg

***Abstract*—We present a formation control algorithm for double-integrator agents, where the formation is time varying and the agents' controls satisfy *a priori* bounds (e.g., the controls can accommodate actuator saturation). We assume that each agent has relative-position-and-velocity feedback of its neighbor agents, where the communication structure is a quasi-strongly connected graph, and at least one agent has a measurement of its position and velocity relative to the leader (if applicable). The main analytic results provide sufficient conditions such that all agents converge to the desired time-varying relative positions with one another and the leader, and have *a priori* bounded controls (if applicable). Next, we extend the formation control algorithm to include collision-avoidance terms that for a set of initial conditions, prevent each agent from colliding with the agents in its neighbor set or colliding with the leader (if applicable). Finally, we present results from rotorcraft experiments that demonstrate the algorithm with time-varying formations and bounded controls. These experimental results include indoor experiments using a motion-capture system as well as outdoor experiments demonstrating the algorithm in a real-world environment with disturbances (e.g., wind) and only onboard feedback.**

I. Introduction

Autonomous multi-vehicle systems have applications in distributed sensing [1], cooperative surveillance [2], precision agriculture, and search and rescue [3]. For example, autonomous multi-aircraft systems could be used in disaster response scenarios such as forest fires or nuclear reactor accidents. In these scenarios, coordinated aircraft could obtain distributed measurements of air quality and atmospheric air flow to plan emergency response. In agriculture, multi-vehicle systems could be used for mapping crops or imaging livestock in pasture for health monitoring. These applications require coordinated control algorithms [4]–[6], which typically rely on sensing and/or communication to provide feedback information, which is used in combination with feedforward data to achieve formation control objectives.

Consensus-based formation control algorithms have been presented for agents with single- and double-integrator dynamics [6]–[18]; more complicated linear dynamics [19]–[22]; nonlinear dynamics [23]–[28]; and rotational dynamics [29]–[34]. These consensus-based algorithms have been studied with a variety of communication (i.e., feedback) structures, including networks that are undirected [15], [16], [20], [35]; directed [17]–[19], [28], [35]; and switching [11], [13], [14], [17], [20], [27], [36]. Sampled-data systems are considered in [8], [9], [16], [17], [28], [35]; and time delays are considered in [8], [11], [16], [21]. Leader-following formation control algorithms have been proposed, where all agents have access to the leader position and velocity (e.g., [7], [10]), and where only some agents have access to the leader position and velocity (e.g., [14], [15], [18], [19], [26]).

Time-varying formations are addressed in in [37]–[39]. However, the algorithms in [37]–[39] do not allow for *a priori* bounded controls. Formation algorithms with *a priori* bounded controls are presented in [40]–[42] using a non-smooth scalar saturation, and in [43] using a smooth scalar saturation. However, none of the algorithms in [40]–[43] allow for time-varying formations. In contrast, [44] presents an algorithm with *a priori* bounded controls that applies to time-varying formations. This algorithm uses a hyperbolic tangent to ensure that the control signal is bounded. However, [44] requires that each agent has acceleration feedback of its neighbors, which is not required in this paper.

This paper addresses leader-following formation control with time-varying formations and bounded controls for agents with double-integrator dynamics. The paper presents several new contributions. First, we introduce a formation control algorithm that addresses time-varying formations and incorporates a formation control function ϕ, which need only belong to a general class of nonlinear functions. For example, ϕ can be selected such that each agent's control is *a priori* bounded, which accommodates actuator magnitude saturation. The function ϕ is more general than those considered in the previous work on *a priori* bounded controls (e.g., [43], [44]). Specifically, the smooth scalar saturation in [43] and the hyperbolic tangent in [44] are special choices of the general function ϕ introduced in this paper. Alternatively, instead of addressing bounded controls, the function ϕ presented in this paper can also be selected such that the magnitudes of the interagent forces increase superlinearly. As a special case, ϕ can also be linear.

Next, we analyze closed-loop stability with the new generalized formation control. For an undirected communication structure, we show that all agents globally converge to the desired time-varying relative positions with one another and the leader (if applicable). In this case, there are no restrictions on the choice of interagent position and velocity gains (provided that the gains are positive). For the case of directed communication, we first show that arbitrary-but-positive interagent gains are not sufficient to guarantee stability even if ϕ is linear. Thus, we provide sufficient conditions on the choice of position and velocity gains for the case where ϕ is linear. Then, the analysis is extended to accommodate nonlinear ϕ. In this case, the stability results are local.

Next, the formation control algorithm is extended to include collision-avoidance terms that for a set of initial conditions, prevent each agent from colliding with the agents in its

Z. S. Lippay and J. B. Hoagg are with the Department of Mechanical Engineering, University of Kentucky, Lexington, KY, USA. (e-mail: zachary.lippay@uky.edu, jesse.hoagg@uky.edu).

This work is supported in part by the U. S. Department of Agriculture (2018-67021-27416), the National Science Foundation (OIA-1849213), and the National Aeronautics and Space Administration (NNX15AR69H) through the NASA Kentucky Space Grant.

neighbor set or the leader (if applicable). Related collision avoidance methods are used in [45]–[48]; however, this paper presents new results by combining collision-avoidance terms with the new formation control algorithm that incorporates ϕ.

Finally, we present results from rotorcraft experiments that demonstrate the formation control algorithm. These experimental results include indoor experiments using a motion capture system as well as outdoor experiments demonstrating the algorithm in a real-world environment with disturbances (e.g., wind) and only onboard feedback (i.e., without a motion-capture system).

II. Notation

Let $x_{(i)}$ denote the ith element of $x \in \mathbb{R}^m$. Let $\|\cdot\|$ be the 2-norm on $\mathbb{R}^m$, and let $\|\cdot\|_\infty$ be the ∞-norm on $\mathbb{R}^m$. Let $1_m \in \mathbb{R}^m$ denote the vector of ones, and let $I_m \in \mathbb{R}^{m\times m}$ denote the $m \times m$ identity matrix. The element in row i and column j of $M \in \mathbb{R}^{m\times m}$ is denoted by $M_{(i,j)}$. Let diag x be the $m \times m$ diagonal matrix whose diagonal elements are the elements of $x \in \mathbb{R}^m$. Let $\otimes$ denote the Kronecker product.

The matrix $M \in \mathbb{R}^{m\times m}$ is *asymptotically stable* if all eigenvalues of M are in the open-left-half plane in $\mathbb{C}$. The matrix $M \in \mathbb{R}^{m\times m}$ is *positive semidefinite* if M is symmetric and for all $x \in \mathbb{R}^m$, $x^{\mathrm{T}}Mx \geq 0$. The matrix $M \in \mathbb{R}^{m\times m}$ is *positive definite* if M is symmetric and for all $x \in \mathbb{R}^m \setminus \{0\}$, $x^{\mathrm{T}}Mx > 0$. Let $\lambda_{\max}(M)$ denote the maximum eigenvalue of the positive-semidefinite matrix $M \in \mathbb{R}^{m\times m}$.

For $m \in \{2, 3\}$, we define the following notation. Let $e_i \in \mathbb{R}^m$ be the ith column of I_m. The special orthogonal group $\mathrm{SO}(m)$ is the set of orthogonal matrices in $\mathbb{R}^{m\times m}$ with determinant one. The set of skew symmetric matrices is denoted $\mathrm{so}(m)$. If $x \in \mathbb{R}^3$, then define

$$[x]_\times \triangleq \begin{bmatrix} 0 & -e_3^{\mathrm{T}}x & e_2^{\mathrm{T}}x \\ e_3^{\mathrm{T}}x & 0 & -e_1^{\mathrm{T}}x \\ -e_2^{\mathrm{T}}x & e_1^{\mathrm{T}}x & 0 \end{bmatrix} \in \mathrm{so}(3).$$

III. Problem Formulation

Let the positive integer n be the number of agents, and define $\mathcal{I} \triangleq \{1, 2, 3, ..., n\}$, which is the agent index set. For each $i \in \mathcal{I}$, consider the double-integrator dynamics

$$\dot{q}_i(t) = p_i(t), \tag{1}$$
$$\dot{p}_i(t) = u_i(t), \tag{2}$$

where $t \geq 0$, $q_i(t) \in \mathbb{R}^m$, $p_i(t) \in \mathbb{R}^m$, and $u_i(t) \in \mathbb{R}^m$ are the position, velocity, and control of the ith agent; and $q_i(0)$ and $p_i(0)$ are the initial conditions.

In addition, consider the leader dynamics

$$\dot{q}_{\mathrm{g}}(t) = p_{\mathrm{g}}(t), \tag{3}$$
$$\dot{p}_{\mathrm{g}}(t) = u_{\mathrm{g}}(t), \tag{4}$$

where $q_{\mathrm{g}}(t) \in \mathbb{R}^m$ and $p_{\mathrm{g}}(t) \in \mathbb{R}^m$ are the position and velocity of the leader; $q_{\mathrm{g}}(0)$ and $p_{\mathrm{g}}(0)$ are the initial conditions; and $u_{\mathrm{g}} : [0, \infty) \to \mathbb{R}^m$ is an exogenous command.

Unless otherwise stated, all statements that involve the subscript i are for all $i \in \mathcal{I}$, and all statements that involve the subscripts i and j are for all $(i, j) \in \mathcal{P} \triangleq \{(i, j) \in \mathcal{I} \times \mathcal{I} \colon i \neq j\}$, which is the set of ordered pairs.

Let $\delta_i : [0, \infty) \to \mathbb{R}^m$ be the time-varying desired position of the ith agent relative to the leader, and define $\delta_{ij} \triangleq \delta_i - \delta_j$, which is the time-varying desired position of the ith agent relative to the jth agent. The objective is to design a control u_i such that:

(O1) For all $(i, j) \in \mathcal{P}$, $\lim_{t\to\infty}[q_i(t) - q_j(t) - \delta_{ij}(t)] = 0$.
(O2) For all $(i, j) \in \mathcal{P}$, $\lim_{t\to\infty}[p_i(t) - p_j(t) - \dot{\delta}_{ij}(t)] = 0$.
(O3) For all $i \in \mathcal{I}$, $\lim_{t\to\infty}[q_i(t) - q_{\mathrm{g}}(t) - \delta_i(t)] = 0$.
(O4) For all $i \in \mathcal{I}$, $\lim_{t\to\infty}[p_i(t) - p_{\mathrm{g}}(t) - \dot{\delta}_i(t)] = 0$.

Objective (O1) states that the interagent positions approach the desired values, and (O3) states that each agent approaches its desired relative position with the leader. Objective (O2) states that the interagent velocities approach the desired values, and (O4) states that each agent approaches its desired relative velocity with the leader. Note that if (O3) is satisfied, then (O1) is satisfied. Similarly, if (O4) is satisfied, then (O2) is satisfied. However, we enumerate these objectives independently because some results in this paper show that a subset of the objectives (e.g., (O1) and (O2)) are satisfied without leader-to-agent communication.

To illustrate one potential application of a formation control algorithm that achieves (O1)–(O4) with time-varying desired positions δ_i, consider a scenario where n robotic agents need to obtain constant-perspective images of an imaging target that is translating and rotating. In this case, the imaging target's position is q_{g}, which ensures that the formation translates with the imaging target. Furthermore, the time-varying desired positions are $\delta_i(t) = R(t)d_i$, where $R(t) \in \mathrm{SO}(3)$ is the rotation matrix from a body frame (that is fixed to and rotates with the imaging target) to the inertial frame, and $d_i \in \mathbb{R}^3$ is the desired position of the ith agent relative to the imaging target resolved in the imaging target's body frame. Thus, the formation translates and rotates with the target, which allows each agent to obtain constant-perspective images of the target.

The interagent communication (i.e., feedback) structure is described using a directed graph. The agent index set $\mathcal{I}$ is the *vertex set*, and the n elements of $\mathcal{I}$ are the *vertices*. Let $\mathcal{E} \subset \mathcal{I} \times \mathcal{I}$ be the *directed edge set*. The elements of $\mathcal{E}$ are the *directed edges*. Then, the directed graph is $\mathcal{G} = (\mathcal{I}, \mathcal{E})$. The directed graph $\mathcal{G} = (\mathcal{I}, \mathcal{E})$ *has a walk of length l from $v_0 \in \mathcal{I}$ to $v_l \in \mathcal{I}$* if there exists an $(l + 1)$-tuple $(v_0, v_1, \ldots, v_l) \in \mathcal{I}\times\mathcal{I}\times\cdots\times\mathcal{I}$ such that for all $j \in \{1, 2, \ldots, l\}$, $(v_{j-1}, v_j) \in \mathcal{E}$. The directed graph $\mathcal{G} = (\mathcal{I}, \mathcal{E})$ is *quasi-strongly connected* if there exists an $\ell \in \mathcal{I}$ such that for all $j \in \mathcal{I} \setminus \{\ell\}$, $\mathcal{G} = (\mathcal{I}, \mathcal{E})$ has a walk from ℓ to j. In this case, ℓ is a *center vertex* of the quasi-strongly connected directed graph $\mathcal{G} = (\mathcal{I}, \mathcal{E})$.

In this paper, we assume that the interagent communication structure is represented by a quasi-strongly connected graph. For many practical applications, the assumption of quasi-strongly connected communication is reasonable because the agents operate in relatively close physical proximity, which facilitates communication. For example, consider the cooperative imaging application discussed above. As another example, consider distributed sensing applications such as airborne plume detection or cooperative crop mapping for precision agriculture. In all of these applications, it is reasonable to have a quasi-strongly connected communication network. How-

ever, if, at some point in time (e.g., initially), the interagent communication network is not quasi-strongly connected, then alternative control logic could be implemented to drive the agents to physical locations where the communication is quasi-strongly connected. At this point, the control can be switched to the algorithm in this paper.

Define the *neighbor set* $\mathcal{N}_i \triangleq \{j \in \mathcal{I} : (j,i) \in \mathcal{E}\}$. Without loss of generality, we assume that for all $i \in \mathcal{I}$, $(i,i) \notin \mathcal{E}$, which implies that $i \notin \mathcal{N}_i$. We assume that $\mathcal{G} = (\mathcal{I}, \mathcal{E})$ is quasi-strongly connected, and the ith agent has access to $\{q_j - q_i\}_{j\in\mathcal{N}_i}$ and $\{p_j - p_i\}_{j\in\mathcal{N}_i}$ for feedback. The results in this paper only require that at least one agent has access to measurements of its position and velocity relative to the leader. We assume that the ith agent has access to measurements of $\ddot{\delta}_i$ and u_{g} for feedforward. In many practical applications such as rotorcraft formation flying, it is reasonable to assume that each agent (e.g., rotorcraft) has access to the required information regarding the leader and time-varying formation through direct measurement and/or communication, or because the leader's maneuvers and the time-varying formation are specified *a priori*. In addition, for practical applications, if u_{g} and $\ddot{\delta}_i$ are relatively small, then the algorithm can be effectively implemented with $u_{\mathrm{g}} = 0$ and $\ddot{\delta}_i = 0$.

IV. Formation Control Algorithm

Let $\Phi : \mathbb{R}^m \to \mathbb{R}$ be positive definite and radially unbounded with $\Phi(0) = 0$. Consider $\phi : \mathbb{R}^m \to \mathbb{R}^m$ defined by

$$\phi(x) \triangleq \left[\frac{\partial \Phi(x)}{\partial x}\right]^{\mathrm{T}},$$

where ϕ satisfies the following conditions:

(C1) ϕ is continuously differentiable.
(C2) For all $x \in \mathbb{R}^m$, $\phi(x) = -\phi(-x)$.
(C3) For all $x \in \mathbb{R}^m \setminus \{0\}$, $x^{\mathrm{T}}\phi(x) > 0$.

The following examples for Φ and ϕ satisfy (C1)–(C3).

Example 1. Let $\Phi(x) = \frac{1}{2}x^{\mathrm{T}}x$. Thus, $\phi(x) = x$. △

Example 2. Let $\Phi(x) = \Big(-1 + \sqrt{1+\nu x^{\mathrm{T}}x}\Big)/\nu$, where $\nu > 0$, which implies that $\phi(x) = (1/\sqrt{1+\nu x^{\mathrm{T}}x})x$. △

Example 3. Let $\Phi(x) = \Big(-m + \sum_{i=1}^m \sqrt{1+\nu x_{(i)}^2}\Big)/\nu$, where $\nu > 0$, which implies that

$$\phi(x) = \left[\begin{array}{ccc} \frac{x_{(1)}}{\sqrt{1+\nu x_{(1)}^2}} & \cdots & \frac{x_{(m)}}{\sqrt{1+\nu x_{(m)}^2}} \end{array}\right]^{\mathrm{T}}. \quad \triangle$$

Example 4. Let $\Phi(x) = \sum_{i=1}^m \log\cosh x_{(i)}$, which implies that $\phi(x) = \left[\begin{array}{ccc}\tanh x_{(1)} & \cdots & \tanh x_{(m)}\end{array}\right]^{\mathrm{T}}$. △

Example 5. Let $\Phi(x) = \frac{1}{2}x^{\mathrm{T}}x + \frac{\nu}{2\eta}(x^{\mathrm{T}}x)^{\eta}$, where $\nu > 0$ and $\eta > 1$. Thus, $\phi(x) = (1 + \nu(x^{\mathrm{T}}x)^{\eta-1})x$. △

The function ϕ in Example 1 is linear, whereas the functions ϕ in Examples 2–4 are sublinear and bounded. Finally, ϕ in Example 5 is superlinear.

To achieve objectives (O1)–(O4), we consider the control

$$u_i \triangleq u_{\mathrm{g}} + \ddot{\delta}_i + a_i\phi(q_{\mathrm{g}} - q_i + \delta_i) + b_i\phi\Big(p_{\mathrm{g}} - p_i + \dot{\delta}_i\Big) + \sum_{j\in\mathcal{N}_i}\Big[\alpha_{ij}\phi(q_j - q_i + \delta_{ij}) + \beta_{ij}\phi\Big(p_j - p_i + \dot{\delta}_{ij}\Big)\Big], \quad (5)$$

where $a_i \geq 0$ and $b_i \geq 0$; for all $j \in \mathcal{N}_i$, $\alpha_{ij} > 0$ and $\beta_{ij} > 0$; and for all $j \notin \mathcal{N}_i$, $\alpha_{ij} = 0$ and $\beta_{ij} = 0$. The results in this paper only require that one agent has access to its position and velocity relative to the leader. Specifically, a_i and b_i need to be positive for at least one agent, which is a center vertex of $\mathcal{G}$.

Notice that if the leader's acceleration $\ddot{u}_{\mathrm{g}}$ and the formation acceleration $\ddot{\delta}_i$ are bounded and ϕ is selected as a bounded function (e.g., Examples 2–4), then it follows from (5) that each term of the control is bounded, which implies that the control (5) is bounded. For many practical applications, u_{g} and $\ddot{\delta}_i$ are bounded. To illustrate how this property can be used to address actuator magnitude saturation, consider a scenario where each element of each agent's control saturates at $\bar{u} > 0$. Thus, we aim to design (5) such that for all $t \geq 0$, $\|u_i(t)\|_\infty \leq \bar{u}$. Assume that u_{g} and $\ddot{\delta}_i$ are bounded. Specifically, assume that there exists $\bar{u}' \in (0, \bar{u})$ such that $t \geq 0$, $\|u_{\mathrm{g}}(t) + \ddot{\delta}_i(t)\|_\infty \leq \bar{u}'$, which is necessary for (5) to satisfy the actuator constraint. Let ϕ be given by Example 4, and let the gains be such that $a_i + b_i + \sum_{j\in\mathcal{N}_i}(\alpha_{ij} + \beta_{ij}) \leq \bar{u} - \bar{u}'$. Thus, it follow from (5) and the triangle inequality that for all $t \geq 0$, $\|u_i(t)\|_\infty \leq \bar{u}' + a_i + b_i + \sum_{j\in\mathcal{N}_i}\big(\alpha_{ij} + \beta_{ij}\big) \leq \bar{u}$, which demonstrates that the actuators do not saturate.

Next, define the position and velocity errors

$$\xi_i \triangleq q_i - q_{\mathrm{g}} - \delta_i, \qquad \rho_i \triangleq p_i - p_{\mathrm{g}} - \dot{\delta}_i, \quad (6)$$

and define $\xi \triangleq \left[\begin{array}{ccc}\xi_1^{\mathrm{T}} & \cdots & \xi_n^{\mathrm{T}}\end{array}\right]^{\mathrm{T}}$ and $\rho \triangleq \left[\begin{array}{ccc}\rho_1^{\mathrm{T}} & \cdots & \rho_n^{\mathrm{T}}\end{array}\right]^{\mathrm{T}}$. Differentiating (6) and using (1)–(5) yields

$$\dot{\xi}_i = \rho_i, \quad (7)$$

$$\dot{\rho}_i = \hat{u}_i, \quad (8)$$

where

$$\hat{u}_i \triangleq -a_i\phi(\xi_i) - b_i\phi(\rho_i) + \sum_{j\in\mathcal{N}_i}\Big[\alpha_{ij}\phi(\xi_j - \xi_i) + \beta_{ij}\phi(\rho_j - \rho_i)\Big]. \quad (9)$$

Note that if there is no leader (i.e., $a_i = b_i = 0$) and ϕ is given by Example 1, then (9) reduces to a standard linear double-integrator consensus algorithm (e.g., [6], [7], [20]) for the error dynamics (7) and (8).

V. Analysis with Undirected Communication

In this section, we analyze the stability of the closed-loop system (7)–(9) with undirected communication (i.e., $\alpha_{ij} = \alpha_{ji}$ and $\beta_{ij} = \beta_{ji}$). The following preliminary result is used to analyze stability. The proof is in Appendix A.

Lemma 1. For all $(i,j) \in \mathcal{P}$, let $a_{ij} = a_{ji} \geq 0$. Then, for all $(x_1, \ldots, x_n, y_1, \ldots, y_n) \in \mathbb{R}^m \times \cdots \times \mathbb{R}^m$,

$$\sum_{(i,j)\in\mathcal{P}} a_{ij}x_i^{\mathrm{T}}\phi(y_j - y_i) = -\sum_{(i,j)\in\mathcal{P}} \frac{a_{ij}}{2}(x_i - x_j)^{\mathrm{T}}\phi(y_i - y_j).$$

The following theorem is the main result that addresses an undirected communication structure. This result shows that

if $\mathcal{G}$ is quasi-strongly connected and at least one agent has a measurement of its position and velocity relative to the leader, then the origin is a globally asymptotically stable equilibrium of (7)–(9), and for all initial conditions, (O1)–(O4) are satisfied. This theorem also provides results where none of the agents have a measurement of their position relative to the leader.

Theorem 1. Consider the closed-loop dynamics (7)–(9), which consists of (1)–(5). Assume that $\mathcal{G} = (\mathcal{I}, \mathcal{E})$ is quasi-strongly connected. For all $(i, j) \in \mathcal{P}$, let $\alpha_{ij} = \alpha_{ji}$ and $\beta_{ij} = \beta_{ji}$. Then, the following statements hold:

i) Assume that for all $i \in \mathcal{I}$, $a_i = 0$ and $b_i = 0$. Then, for all $(\xi(0), \rho(0)) \in \mathbb{R}^{2mn}$, (O1) and (O2) are satisfied.

ii) Assume that there exists $\ell \in \mathcal{I}$ such that $b_\ell > 0$. Then, for all $(\xi(0), \rho(0)) \in \mathbb{R}^{2mn}$, (O1), (O2), and (O4) are satisfied.

iii) Assume that there exist $\ell_1, \ell_2 \in \mathcal{I}$ such that $a_{\ell_1} > 0$ and $b_{\ell_2} > 0$. Then, the origin is a globally asymptotically stable equilibrium of (7)–(9), and for all $(\xi(0), \rho(0)) \in \mathbb{R}^{2mn}$, (O1)–(O4) are satisfied.

Prior to proving Theorem 1, we briefly outline the approach used in the proof. To show i), we use a Lyapunov-like function to demonstrate that (O2) is satisfied and $\xi_i - \xi_j$ is bounded. Next, we use Barbalat's lemma to show that the difference in acceleration $\dot\rho_i - \dot\rho_j$ converges to zero, which is used in combination with (O2) and boundedness of $\xi_i - \xi_j$ to show that (O1) is satisfied. Similar approaches are used to demonstrate that (O3) and (O4) are satisfied (if applicable).

Proof of Theorem 1: Consider the Lyapunov-like function $V : \mathbb{R}^{mn} \times \mathbb{R}^{mn} \to [0, \infty)$ defined by

$$V(\xi, \rho) \triangleq \sum_{i \in \mathcal{I}} \Big[a_i \Phi(\xi_i) + \frac{1}{2} \rho_i^{\mathrm{T}} \rho_i + \sum_{j \in \mathcal{N}_i} \frac{\alpha_{ij}}{2} \Phi(\xi_i - \xi_j) \Big]. \quad (10)$$

Since Φ is positive definite, it follows that V is nonnegative. Next, define

$$\dot V(\xi, \rho) \triangleq \sum_{i \in \mathcal{I}} \left[\frac{\partial V}{\partial \xi_i} \dot\xi_i + \frac{\partial V}{\partial \rho_i} \dot\rho_i \right] = \sum_{i \in \mathcal{I}} \Big[a_i \phi^{\mathrm{T}}(\xi_i) \dot\xi_i + \rho_i^{\mathrm{T}} \dot\rho_i + \sum_{j \in \mathcal{N}_i} \frac{\alpha_{ij}}{2} \phi^{\mathrm{T}}(\xi_i - \xi_j)(\dot\xi_i - \dot\xi_j) \Big],$$

and evaluating $\dot V$ along the trajectories of (7)–(9) yields

$$\dot V = \sum_{i \in \mathcal{I}} \Big[- b_i \rho_i^{\mathrm{T}} \phi(\rho_i) + \sum_{j \in \mathcal{N}_i} \Big[\alpha_{ij} \rho_i^{\mathrm{T}} \phi(\xi_j - \xi_i) + \beta_{ij} \rho_i^{\mathrm{T}} \phi(\rho_j - \rho_i) + \frac{\alpha_{ij}}{2} (\rho_i - \rho_j)^{\mathrm{T}} \phi(\xi_i - \xi_j) \Big] \Big],$$

where we omit the arguments from $\dot V$. Since for all $j \notin \mathcal{N}_i$, $\alpha_{ij} = 0$ and $\beta_{ij} = 0$, it follows that

$$\dot V = \sum_{i \in \mathcal{I}} - b_i \rho_i^{\mathrm{T}} \phi(\rho_i) + \sum_{(i,j) \in \mathcal{P}} \Big[\alpha_{ij} \rho_i^{\mathrm{T}} \phi(\xi_j - \xi_i) + \beta_{ij} \rho_i^{\mathrm{T}} \phi(\rho_j - \rho_i) + \frac{\alpha_{ij}}{2} (\rho_i - \rho_j)^{\mathrm{T}} \phi(\xi_i - \xi_j) \Big].$$

Since $\alpha_{ij} = \alpha_{ji}$ and $\beta_{ij} = \beta_{ji}$, using Lemma 1 implies that

$$\begin{aligned} \dot V &= - \sum_{i \in \mathcal{I}} b_i \rho_i^{\mathrm{T}} \phi(\rho_i) - \sum_{(i,j) \in \mathcal{P}} \frac{\beta_{ij}}{2} (\rho_i - \rho_j)^{\mathrm{T}} \phi(\rho_i - \rho_j) \\ &= - \sum_{i \in \mathcal{I}} \Big[b_i \rho_i^{\mathrm{T}} \phi(\rho_i) + \sum_{j \in \mathcal{N}_i} \frac{\beta_{ij}}{2} (\rho_i - \rho_j)^{\mathrm{T}} \phi(\rho_i - \rho_j) \Big], \end{aligned} \quad (11)$$

and (C3) implies that $\dot V$ is nonpositive. Thus, V is bounded, and it follows from (10) that ρ_i is bounded; for all $i \in \mathcal{I}_a \triangleq \{i \in \mathcal{I} \colon a_i > 0\}$, $\Phi(\xi_i)$ is bounded; and for all $(i, j) \in \mathcal{I} \times \mathcal{N}_i$, $\Phi(\xi_i - \xi_j)$ is bounded. Since, $\mathcal{G}$ is quasi-strongly connected and for all $(i, j) \in \mathcal{I} \times \mathcal{N}_i$, $\Phi(\xi_i - \xi_j)$ is bounded, it follows that $\Phi(\xi_i - \xi_j)$ is bounded. Since, in addition, Φ is positive definite and radially unbounded, it follows that $\xi_i - \xi_j$ is bounded, and for all $i \in \mathcal{I}_a$, ξ_i is bounded.

Define $\mathcal{I}_b \triangleq \{i \in \mathcal{I} \colon b_i > 0\}$ and $H \triangleq \{(\xi, \rho) \in \mathbb{R}^{2mn} \colon \dot V(\xi, \rho) = 0\}$, and it follows from (11) and (C3) that $H = \{(\xi, \rho) \in \mathbb{R}^{2mn} \colon$ for all $i \in \mathcal{I}_b$, $\rho_i = 0$ and for all $(i, j) \in \mathcal{I} \times \mathcal{N}_i$, $\rho_i - \rho_j = 0\}$. LaSalle's invariance theorem implies that $(\xi(t), \rho(t))$ converges to H. Thus, for all $i \in \mathcal{I}_b$, $\lim_{t \to \infty} \rho_i(t) = 0$, and for all $(i, j) \in \mathcal{I} \times \mathcal{N}_i$, $\lim_{t \to \infty} [\rho_i(t) - \rho_j(t)] = 0$. Since, in addition, $\mathcal{G}$ is quasi-strongly connected, it follows that $\lim_{t \to \infty} [\rho_i(t) - \rho_j(t)] = 0$. Thus, $\lim_{t \to \infty} [p_i(t) - p_j(t) - \dot\delta_{ij}(t)] = 0$, which confirms that (O2) is satisfied.

Next, consider $\phi' : \mathbb{R}^m \to \mathbb{R}^{m \times m}$ defined by $\phi'(x) \triangleq \frac{\partial \phi(x)}{\partial x}$, and note that (C1) implies that ϕ' is continuous. Differentiating (8) and using (9) implies that

$$\ddot\rho_i = -a_i \phi'(\xi_i) \rho_i - b_i \phi'(\rho_i) \hat u_i + \sum_{j \in \mathcal{N}_i} \Big[\alpha_{ij} \phi'(\xi_j - \xi_i) \times (\rho_j - \rho_i) + \phi'(\rho_j - \rho_i)(\hat u_j - \hat u_i) \Big], \quad (12)$$

and note that (9) implies that $\hat u_i$ is bounded because ρ_i, $\xi_i - \xi_j$, and $\{\xi_i\}_{i \in \mathcal{I}_a}$ are bounded. Since $\hat u_i$, ρ_i, $\xi_i - \xi_j$, and $\{\xi_i\}_{i \in \mathcal{I}_a}$ are bounded, it follows from (12) that $\ddot\rho_i$ is bounded, which implies that $\dot\rho_i$ is uniformly continuous.

Since for all $j \notin \mathcal{N}_i$, $\alpha_{ij} = 0$ and $\beta_{ij} = 0$, it follows from (8) and (9) that

$$\begin{aligned} - \sum_{i \in \mathcal{I}} \xi_i^{\mathrm{T}} \dot\rho_i &= \sum_{i \in \mathcal{I}} \xi_i^{\mathrm{T}} \Big[a_i \phi(\xi_i) + b_i \phi(\rho_i) - \sum_{j \in \mathcal{N}_i} \Big[\alpha_{ij} \phi(\xi_j - \xi_i) + \beta_{ij} \phi(\rho_j - \rho_i) \Big] \Big] \\ &= \sum_{i \in \mathcal{I}_a} a_i \xi_i^{\mathrm{T}} \phi(\xi_i) + \sum_{i \in \mathcal{I}_b} b_i \xi_i^{\mathrm{T}} \phi(\rho_i) - \sum_{(i,j) \in \mathcal{P}} \Big[\alpha_{ij} \xi_i^{\mathrm{T}} \phi(\xi_j - \xi_i) + \beta_{ij} \xi_i^{\mathrm{T}} \phi(\rho_j - \rho_i) \Big], \end{aligned} \quad (13)$$

and using Lemma 1 implies that

$$- \sum_{i \in \mathcal{I}} \xi_i^{\mathrm{T}} \dot\rho_i = \sum_{i \in \mathcal{I}_a} a_i \xi_i^{\mathrm{T}} \phi(\xi_i) + \sum_{i \in \mathcal{I}_b} b_i \xi_i^{\mathrm{T}} \phi(\rho_i) + \sum_{(i,j) \in \mathcal{I} \times \mathcal{N}_i} \Big[\frac{\alpha_{ij}}{2} (\xi_i - \xi_j)^{\mathrm{T}} \phi(\xi_i - \xi_j)$$

$$+\frac{\beta_{ij}}{2}(\xi_i-\xi_j)^{\mathrm{T}}\phi(\rho_i-\rho_j)\Big]. \tag{14}$$

To show iii), assume that there exist $\ell_1,\ell_2\in\mathcal{I}$ such that $a_{\ell_1}>0$ and $b_{\ell_2}>0$. Since $\lim_{t\to\infty}\rho_{\ell_2}(t)=0$, and $\lim_{t\to\infty}[\rho_i(t)-\rho_j(t)]=0$, it follows that $\lim_{t\to\infty}\rho_i(t)=0$, which confirms (O4). Since $\lim_{t\to\infty}\int_0^t\dot\rho_i(\tau)\,\mathrm{d}\tau=\lim_{t\to\infty}\rho_i(t)$ exists and $\dot\rho_i$ is uniformly continuous, it follows from Barbalat's Lemma [49, Lemma 8.2] that $\lim_{t\to\infty}\dot\rho_i(t)=0$. Since ξ_{ℓ_1} is bounded and $\xi_i-\xi_j$ is bounded, it follows that ξ_i is bounded. Thus, $\lim_{t\to\infty}\sum_{i\in\mathcal{I}}\xi_i^{\mathrm{T}}(t)\dot\rho_i(t)=0$. Since, in addition, $\lim_{t\to\infty}\rho_i(t)=0$, taking the limit as $t\to\infty$ of (14) implies

$$0=\lim_{t\to\infty}\Bigg[\sum_{(i,j)\in\mathcal{I}\times\mathcal{N}_i}\frac{\alpha_{ij}}{2}(\xi_i(t)-\xi_j(t))^{\mathrm{T}}\phi(\xi_i(t)-\xi_j(t))+\sum_{i\in\mathcal{I}_a}a_i\xi_i^{\mathrm{T}}(t)\phi(\xi_i(t))\Bigg], \tag{15}$$

where it follows from (C3) that every term in (15) is nonnegative, and thus, converge to zero. Thus, $\lim_{t\to\infty}\xi_{\ell_1}(t)=0$ and for all $(i,j)\in\mathcal{I}\times\mathcal{N}_i,\lim_{t\to\infty}[\xi_i(t)-\xi_j(t)]=0$. Since, in addition, $\mathcal{G}$ is quasi-strongly connected, it follows that $\lim_{t\to\infty}[\xi_i(t)-\xi_j(t)]=0$, which confirms (O1). Since, in addition, $\lim_{t\to\infty}\xi_{\ell_1}(t)=0$, it follows that $\lim_{t\to\infty}\xi_i(t)=0$, which confirms (O3). Thus, (O1)–(O4) are satisfied. Since $a_{\ell_1}>0$, (10) implies that V is positive definite, which implies that the origin is a Lyapunov stable equilibrium of (7)–(9) because $\dot V$ is nonpositive. Since, in addition, $\lim_{t\to\infty}\xi_i(t)=0$ and $\lim_{t\to\infty}\rho_i(t)=0$, it follows that the origin is a globally asymptotically stable equilibrium, which verifies iii).

To show i) and ii), assume without loss of generality that $a_i=0$. Consider $W:\mathbb{R}^{mn}\times\mathbb{R}^{mn}\to\mathbb{R}$ defined by

$$W(\xi,\dot\rho)\triangleq-\frac{1}{2}\sum_{(i,j)\in\mathcal{P}}(\xi_i-\xi_j)^{\mathrm{T}}(\dot\rho_i-\dot\rho_j)=\sum_{(i,j)\in\mathcal{I}\times\mathcal{I}}\xi_j^{\mathrm{T}}\dot\rho_i-n\sum_{i\in\mathcal{I}}\xi_i^{\mathrm{T}}\dot\rho_i. \tag{16}$$

Since $a_i=0$ and for all $j\notin\mathcal{N}_i$, $\alpha_{ij}=0$ and $\beta_{ij}=0$, it follows from (8) and (9) that

$$\sum_{i\in\mathcal{I}}\dot\rho_i=-\sum_{i\in\mathcal{I}_b}b_i\phi(\rho_i)+\sum_{(i,l)\in\mathcal{P}}\Big[\alpha_{il}\phi(\xi_l-\xi_i)+\beta_{il}\phi(\rho_l-\rho_i)\Big], \tag{17}$$

Since $\alpha_{ij}=\alpha_{ji}$ and $\beta_{ij}=\beta_{ji}$, it follows from (17) and (C2) that $\sum_{i\in\mathcal{I}}\dot\rho_i=-\sum_{i\in\mathcal{I}_b}b_i\phi(\rho_i)$, which implies that

$$\sum_{(i,j)\in\mathcal{I}\times\mathcal{I}}\xi_j^{\mathrm{T}}\dot\rho_i=-\sum_{(i,j)\in\mathcal{I}_b\times\mathcal{I}}b_i\xi_j^{\mathrm{T}}\phi(\rho_i). \tag{18}$$

Noting that $n\sum_{i\in\mathcal{I}_b}b_i\xi_i^{\mathrm{T}}\phi(\rho_i)-\sum_{(i,j)\in\mathcal{I}_b\times\mathcal{I}}b_i\xi_j^{\mathrm{T}}\phi(\rho_i)=\sum_{(i,j)\in\mathcal{I}_b\times\mathcal{I}}b_i(\xi_i-\xi_j)^{\mathrm{T}}\phi(\rho_i)$, it follows that substituting (14) and (18) into (16) yields

$$W=\sum_{(i,j)\in\mathcal{I}_b\times\mathcal{I}}b_i(\xi_i-\xi_j)^{\mathrm{T}}\phi(\rho_i)+n\sum_{(i,j)\in\mathcal{I}\times\mathcal{N}_i}\Big[\frac{\alpha_{ij}}{2}(\xi_i-\xi_j)^{\mathrm{T}}\times\phi(\xi_i-\xi_j)+\frac{\beta_{ij}}{2}(\xi_i-\xi_j)^{\mathrm{T}}\phi(\rho_i-\rho_j)\Big], \tag{19}$$

where we omit the arguments from W.

Since $\lim_{t\to\infty}\int_0^t\dot\rho_i(\tau)-\dot\rho_j(\tau)\,\mathrm{d}\tau=\lim_{t\to\infty}[\rho_i(t)-\rho_j(t)]$ exists and $\dot\rho_i-\dot\rho_j$ is uniformly continuous, it follows from Barbalat's Lemma that $\lim_{t\to\infty}[\dot\rho_i(t)-\dot\rho_j(t)]=0$. Since, in addition, $\xi_i-\xi_j$ is bounded, it follows from (16) that $\lim_{t\to\infty}W(\xi(t),\dot\rho(t))=0$. Since, in addition, $\lim_{t\to\infty}[\rho_i(t)-\rho_j(t)]=0$ and for all $i\in\mathcal{I}_b$, $\lim_{t\to\infty}\rho_i(t)=0$, taking the limit as $t\to\infty$ of (19) implies that

$$0=\lim_{t\to\infty}\sum_{(i,j)\in\mathcal{I}\times\mathcal{N}_i}\alpha_{ij}(\xi_i(t)-\xi_j(t))^{\mathrm{T}}\phi(\xi_i(t)-\xi_j(t)), \tag{20}$$

where it follows from (C3) that every term in (20) is nonnegative, and thus, converge to zero. Thus, for all $(i,j)\in\mathcal{I}\times\mathcal{N}_i,\lim_{t\to\infty}[\xi_i(t)-\xi_j(t)]=0$. Since, in addition, $\mathcal{G}$ is quasi-strongly connected, it follows that $\lim_{t\to\infty}[\xi_i(t)-\xi_j(t)]=0$, which confirms (O1), and thus, verifies i).

To show ii), assume that there exists $\ell\in\mathcal{I}$ such that $b_\ell>0$. Since $\lim_{t\to\infty}\rho_\ell(t)=0$, and $\lim_{t\to\infty}[\rho_i(t)-\rho_j(t)]=0$, it follows that $\lim_{t\to\infty}\rho_i(t)=0$, which confirms (O4), and thus, verifies ii). ■

The following numerical example demonstrates Theorem 1, where only one agent has measurements of q_i-q_g and p_i-p_g, the leader is translating, and the formation is time varying.

Simulation 1. Let $n=4$ and $m=3$, and let ϕ be given by Example 4. Let $\mathcal{N}_1=\{2,4\}$, $\mathcal{N}_2=\{1,3\}$, $\mathcal{N}_3=\{2,4\}$, and $\mathcal{N}_4=\{1,3\}$, which represents an undirected cyclic feedback structure. For all $j\in\mathcal{N}_i$, let $\alpha_{ij}=1.2$ and $\beta_{ij}=3.5$. Let $a_1=1.5$, $b_1=4.5$, $a_2=a_3=a_4=0$, and $b_2=b_3=b_4=0$. Thus, only the first agent has measurements of its position and velocity relative to the leader. Define $\upsilon(t)\triangleq\cos\pi t/5$, and the time-varying desired positions are $\delta_1(t)=[\,2+\upsilon(t)\quad 2+\upsilon(t+\pi/2)\quad 0\,]^{\mathrm{T}}$ m, $\delta_2(t)=[\,2+\upsilon(t)\quad -2+\upsilon(t+\pi/2)\quad -1\,]^{\mathrm{T}}$ m, $\delta_3(t)=[\,-1+\upsilon(t+\pi/2)\quad \upsilon(t)\quad 3\,]^{\mathrm{T}}$ m, and $\delta_4(t)=[\,\upsilon(t)\quad \upsilon(t+\pi/2)\quad -3\,]^{\mathrm{T}}$ m. The leader's position is

$$q_{\mathrm{g}}(t)=\begin{bmatrix}5\cos\frac{\pi t}{15} & -5\sin\frac{\pi t}{15} & 2\end{bmatrix}^{\mathrm{T}}\text{ m}. \tag{21}$$

Figure 1 shows the three-dimensional agent trajectories q_i and the desired trajectories $q_{\mathrm{g}}+\delta_i$ from $t_1=15$ s to $t_2=30$ s. At $t_1=15$ s the agents are not in the desired time-varying formation; however, by $t_2=30$ s, the agents achieve and maintain the desired time-varying formation. Figures 2 and 3 show that $\lim_{t\to\infty}\xi_i(t)=0$ and $\lim_{t\to\infty}\rho_i(t)=0$, which demonstrates that (O1)–(O4) are satisfied. △

VI. Analysis with Directed Communication

Theorem 1 shows that for undirected communication, the control (5) achieves (O1)–(O4) if $\mathcal{G}$ is quasi-strongly connected and has a center vertex $\ell\in\mathcal{I}$ such that $a_\ell>0$ and $b_\ell>0$. Note that for undirected communication, every vertex is a center vertex. However, Theorem 1 does not require any relationship between the interagent position gains α_{ij} and the interagent velocity gains β_{ij}, or between the agent-leader position gains a_i and the agent-leader velocity gains b_i.

In this section, we first show that for directed communication, the assumptions from the undirected case are not sufficient to ensure that (O1)–(O4) are satisfied. More specifically, it is not sufficient to assume that $\mathcal{G}$ is quasi-strongly connected

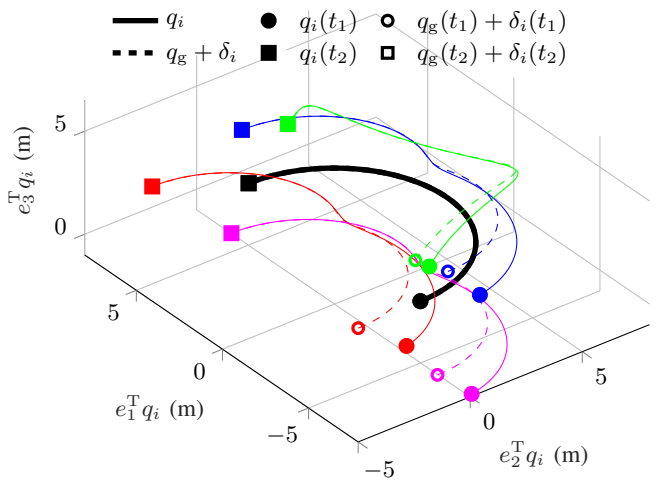

Fig. 1. Three-dimensional agent position q_i and desired time-varying position $q_g + \delta_i$ from $t_1 = 15$ s to $t_2 = 30$ s for agents $i = 1$ (blue), $i = 2$ (red), $i = 3$ (green), and $i = 4$ (magenta). The leader trajectory q_g is shown in black. By $t_2 = 30$ s, the agents achieve the desired time-varying formation.

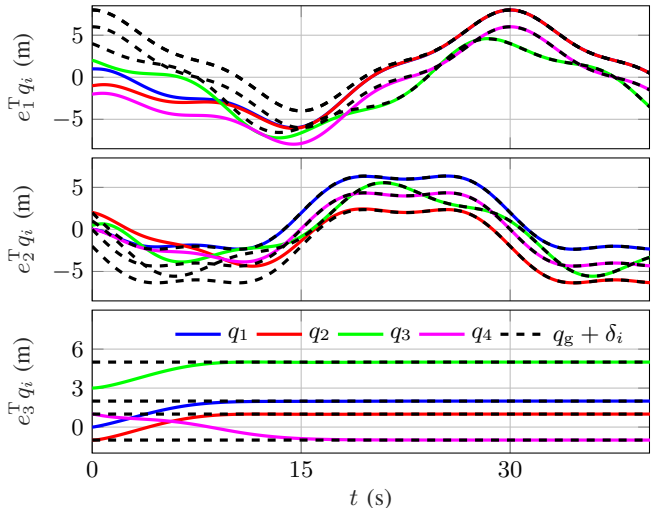

Fig. 2. Position q_i and desired position $q_g + \delta_i$. (O1) and (O3) are satisfied.

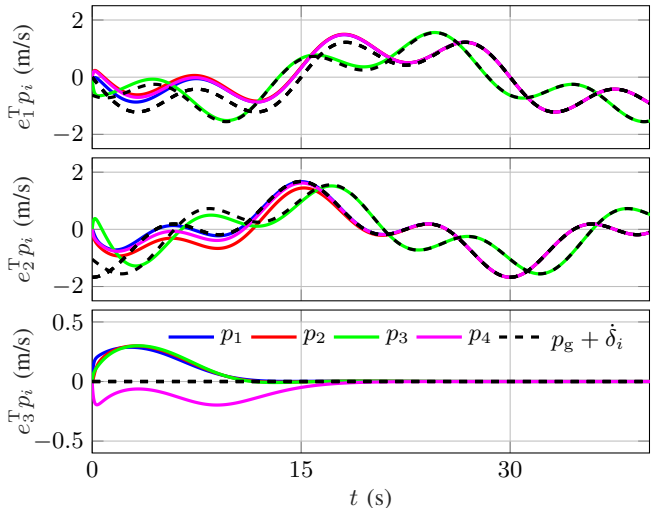

Fig. 3. Velocity p_i and desired velocity $p_g + \dot{\delta}_i$. (O2) and (O4) are satisfied.

and has a center vertex $\ell \in \mathcal{I}$ such that $a_\ell > 0$ and $b_\ell > 0$. In fact, without additional assumptions on the magnitude of the velocity gains b_i and β_{ij} relative to the magnitude of position gains a_i and α_{ij}, the closed-loop dynamics (7)–(9) can be unstable. Therefore, we provide sufficient conditions on choice of the position and velocity gains such that (O1)–(O4) are satisfied for the case where ϕ is linear. Next, we use this linear stability result to provide sufficient conditions on choice of the position and velocity gains such that (O1)–(O4) are satisfied locally for the case where ϕ is nonlinear.

We require the following notation. Let $\mathcal{A}, \mathcal{B} \in \mathbb{R}^{n\times n}$ be such that $\mathcal{A}_{(i,j)} = -\alpha_{ij}$ and $\mathcal{B}_{(i,j)} = -\beta_{ij}$, and $\mathcal{A}_{(i,i)} = \sum_{j\in\mathcal{N}_i} \alpha_{ij}$ and $\mathcal{B}_{(i,i)} = \sum_{j\in\mathcal{N}_i} \beta_{ij}$. Thus, $\mathcal{A}$ and $\mathcal{B}$ are Laplacians of the directed graph $\mathcal{G} = (\mathcal{I}, \mathcal{E})$, where for all $(i, j) \in \mathcal{E}$, we associate the weight α_{ij} and β_{ij}, respectively. Define $\mathcal{A}_\mathrm{d} \triangleq \operatorname{diag}\left[\begin{array}{cccc} a_1 & a_2 & \cdots & a_n \end{array}\right]^\mathrm{T} \in \mathbb{R}^{n\times n}$ and $\mathcal{B}_\mathrm{d} \triangleq \operatorname{diag}\left[\begin{array}{cccc} b_1 & b_2 & \cdots & b_n \end{array}\right]^\mathrm{T} \in \mathbb{R}^{n\times n}$.

The following result provides sufficient conditions such that $\mathcal{A} + \mathcal{A}_\mathrm{d}$ is nonsingular. The proof is in Appendix A.

Lemma 2. Assume that $\mathcal{G} = (\mathcal{I}, \mathcal{E})$ is quasi-strongly connected, and assume that there exists a center vertex $\ell \in \mathcal{I}$ of $\mathcal{G} = (\mathcal{I}, \mathcal{E})$ such that $a_\ell > 0$. Then, $\mathcal{A} + \mathcal{A}_\mathrm{d}$ is nonsingular.

Lemma 2 provides sufficient conditions such that $\mathcal{A}+\mathcal{A}_\mathrm{d}$ is nonsingular; however, these conditions are not necessary. For example, if for all $i \in \mathcal{I}$, $a_i > 0$, then $\mathcal{A} + \mathcal{A}_\mathrm{d}$ is nonsingular. This situation arises if each agent has a measurement of its position relative to the leader. As another example, if $\mathcal{G}$ is the union of k quasi-strongly connected graphs and each one has a center vertex $\ell_1, \ldots, \ell_k \in \mathcal{I}$ such that $a_{\ell_1}, \ldots, a_{\ell_k} > 0$, then $\mathcal{A} + \mathcal{A}_\mathrm{d}$ is nonsingular [50, Lemma 1].

The results in this section rely on the assumption that $\mathcal{A} + \mathcal{A}_\mathrm{d}$ is nonsingular, and Lemma 2 provides one communication (i.e., feedback) structure under which $\mathcal{A} + \mathcal{A}_\mathrm{d}$ is nonsingular. However, the results in this section apply to all communication structures such that $\mathcal{A} + \mathcal{A}_\mathrm{d}$ is nonsingular.

The following example considers a scenario where $\mathcal{G}$ is quasi-strongly connected and has a center vertex $\ell \in \mathcal{I}$ such that $a_\ell > 0$ and $b_\ell > 0$. For undirected communication these conditions are sufficient to guarantee that the origin of (7)–(9) is globally asymptotically stable and (O1)–(O4) are satisfied. However, this next example demonstrates that for directed communication, the origin of (7)–(9) can be unstable without additional assumptions on the position and velocity gains.

Example 6. Let ϕ be such that $\frac{\partial \phi(x)}{\partial x}|_{x=0} = \phi_0 I_m$, where $\phi_0 > 0$. Examples 1–5 for ϕ satisfy this condition with $\phi_0 = 1$. Let $n = 4$ and $m = 1$. Let $\mathcal{N}_1 = \{2\}$, $\mathcal{N}_2 = \{3\}$, $\mathcal{N}_3 = \{4\}$, and $\mathcal{N}_4 = \{1\}$, which represents a directed cyclic feedback structure. For all $j \in \mathcal{N}_i$, let $\alpha_{ij} = 1/\phi_0$ and $\beta_{ij} = 0.3\alpha_{ij}$. Let $a_1 = 2/\phi_0$, $b_1 = 0.3a_1$, $a_2 = a_3 = a_4 = 0$, and $b_2 = b_3 = b_4 = 0$, which implies that the first agent has measurements of its position and velocity relative to the leader. In this case, $\mathcal{G}$ is quasi-strongly connected and has the center vertex $\ell = 1$ such that $a_\ell > 0$ and $b_\ell > 0$. Lemma 2 implies that $\mathcal{A} + \mathcal{A}_\mathrm{d}$ and $\mathcal{B} + \mathcal{B}_\mathrm{d}$ are nonsingular. It follows from direct calculation

that the linearization of (7)–(9) about the origin is given by

$$\begin{bmatrix} \dot{\xi} \\ \dot{\rho} \end{bmatrix} = A \begin{bmatrix} \xi \\ \rho \end{bmatrix},$$

where

$$A \triangleq \begin{bmatrix} 0_{4\times4} & I_4 \\ A_{21} & 0.3A_{21} \end{bmatrix}, \quad A_{21} \triangleq \begin{bmatrix} -3 & 1 & 0 & 0 \\ 0 & -1 & 1 & 0 \\ 0 & 0 & -1 & 1 \\ 1 & 0 & 0 & -1 \end{bmatrix}.$$

In this case, A has 6 eigenvalues in the open-left-half plane and 2 eigenvalues in the open-right-half plane, which are $0.1075 \pm \jmath 1.2842$. Thus, Lyapunov's indirect method implies that the origin of (7)–(9) is an unstable equilibrium. △

Note that the closed-loop dynamics in Example 6 are unstable even if the control (5) is linear (i.e., ϕ is given by Example 1). Also, note that in Example 6 the velocity gains are proportional to the position gains, specifically, $b_i = \kappa a_i$ and $\beta_{ij} = \kappa\alpha_{ij}$, where $\kappa = 0.3$. However, this is not sufficient to ensure closed-loop stability with directed communication.

The following result is used to analyze stability with directed communication. This result is given in [18, Lemma 4].

Lemma 3. Assume that $\mathcal{A}+\mathcal{A}_{\mathrm{d}}$ is nonsingular. Then, $D \triangleq \operatorname{diag}\left[(\mathcal{A}+\mathcal{A}_{\mathrm{d}})^{-\mathrm{T}}1_n\right]$ and $Q \triangleq (\mathcal{A}+\mathcal{A}_{\mathrm{d}})^{\mathrm{T}}D + D(\mathcal{A}+\mathcal{A}_{\mathrm{d}})$ are positive definite.

For the moment, assume that ϕ is linear (i.e., $\phi(x) = \phi_0 x$ where $\phi_0 > 0$). In this case, it follows from (7)–(9) that

$$\begin{bmatrix} \dot{\xi} \\ \dot{\rho} \end{bmatrix} = A \begin{bmatrix} \xi \\ \rho \end{bmatrix}, \tag{22}$$

where

$$A \triangleq \begin{bmatrix} 0_{n\times n} & I_n \\ -\phi_0(\mathcal{A}+\mathcal{A}_{\mathrm{d}}) & -\phi_0(\mathcal{B}+\mathcal{B}_{\mathrm{d}}) \end{bmatrix} \otimes I_m. \tag{23}$$

The following result addresses the case where the communication is directed and ϕ is linear. This result provides sufficient conditions such that A is asymptotically stable, and (O1)–(O4) are satisfied.

Proposition 1. Consider the closed-loop dynamics (22) and (23), which consists of (1)–(5), where $\phi(x) = \phi_0 x$ and $\phi_0 > 0$. Assume that $\mathcal{A}+\mathcal{A}_{\mathrm{d}}$ is nonsingular. Let $D \in \mathbb{R}^{n\times n}$ be the positive-definite diagonal matrix given by Lemma 3, and let $Q \in \mathbb{R}^{n\times n}$ be the positive-definite matrix given by Lemma 3. Furthermore, let

$$\kappa > \sqrt{\frac{2}{\phi_0}\lambda_{\max}\left(D^{\frac{1}{2}}Q^{-1}D^{\frac{1}{2}}\right)} \in (0,\infty). \tag{24}$$

For all $i \in \mathcal{I}$, let $b_i = \kappa a_i$, and for all $(i,j) \in \mathcal{P}$, let $\beta_{ij} = \kappa\alpha_{ij}$. Then, A is asymptotically stable, and for all $(\xi(0),\rho(0)) \in \mathbb{R}^{2mn}$, (O1)–(O4) are satisfied.

Proof: Define $P \triangleq \hat{P} \otimes I_m \in \mathbb{R}^{mn\times mn}$, where

$$\hat{P} \triangleq \frac{1}{\phi_0}\begin{bmatrix} D & \frac{\kappa}{2}D \\ \frac{\kappa}{2}D & \frac{\kappa^2}{2}D \end{bmatrix}.$$

The Schur complement of $\hat{P}$ with respect to D is $\hat{P}_{\mathrm{c}} \triangleq \frac{1}{\phi_0}(\frac{\kappa^2}{2}D - (\frac{\kappa}{2}D)D^{-1}(\frac{\kappa}{2}D)) = \frac{\kappa^2}{4\phi_0}D$. Since D and $\hat{P}_{\mathrm{c}}$ are positive definite, it follows from [51, Prop. 8.2.4] that $\hat{P}$ is positive definite, which implies that P is positive definite.

Since $b_i = \kappa a_i$, and for all $(i,j) \in \mathcal{P}$, $\beta_{ij} = \kappa\alpha_{ij}$, it follows from (23) that

$$A = \begin{bmatrix} 0_{n\times n} & I_n \\ -\phi_0(\mathcal{A}+\mathcal{A}_{\mathrm{d}}) & -\kappa\phi_0(\mathcal{A}+\mathcal{A}_{\mathrm{d}}) \end{bmatrix} \otimes I_m,$$

which implies that

$$T \triangleq -A^{\mathrm{T}}P - PA = \hat{T} \otimes I_m, \tag{25}$$

where

$$\hat{T} \triangleq \begin{bmatrix} \frac{\kappa}{2}Q & \frac{\kappa^2}{2}Q - \frac{1}{\phi_0}D \\ \frac{\kappa^2}{2}Q - \frac{1}{\phi_0}D & \frac{\kappa^3}{2}Q - \frac{\kappa}{\phi_0}D \end{bmatrix}.$$

The Schur complement of $\hat{T}$ with respect to $\frac{\kappa}{2}Q$ is

$$\begin{aligned}\hat{T}_{\mathrm{c}} &\triangleq \frac{\kappa^3}{2}Q - \frac{\kappa}{\phi_0}D - \left(\frac{\kappa^2}{2}Q - \frac{D}{\phi_0}\right)\left(\frac{\kappa}{2}Q\right)^{-1}\left(\frac{\kappa^2}{2}Q - \frac{D}{\phi_0}\right) \\ &= \frac{\kappa}{\phi_0}D - \frac{2}{\kappa\phi_0^2}DQ^{-1}D. \end{aligned}\tag{26}$$

Next, since Q and D are positive definite, it follows from (24) that $\kappa^2 - \frac{2}{\phi_o}\lambda_{\max}(D^{\frac{1}{2}}Q^{-1}D^{\frac{1}{2}}) > 0$. Thus, $\frac{\kappa}{\phi_0}D - \frac{2}{\kappa\phi_0}\lambda_{\max}(D^{\frac{1}{2}}Q^{-1}D^{\frac{1}{2}})D$ is positive definite, which combined with (26) implies that $\hat{T}_{\mathrm{c}}$ is positive definite. Since $\frac{\kappa}{2}Q$ and $\hat{T}_{\mathrm{c}}$ are positive definite, it follows from [51, Prop. 8.2.4] that $\hat{T}$ is positive definite, which implies that T is positive definite. Since P and T are positive definite, it follows from (25) that A is asymptotically stable.

Since A is asymptotically stable, it follows from (22) that $\lim_{t\to\infty}\xi(t) = 0$ and $\lim_{t\to\infty}\rho(t) = 0$. Thus, $\lim_{t\to\infty}\rho_i(t) = 0$ and $\lim_{t\to\infty}[\rho_i(t) - \rho_j(t)] = 0$, which confirms (O4) and (O2) are satisfied. Since $\lim_{t\to\infty}\xi(t) = 0$, it follows that $\lim_{t\to\infty}[q_i(t) - q_{\mathrm{g}}(t) - \delta_i(t)] = \lim_{t\to\infty}\xi_i(t) = 0$ and $\lim_{t\to\infty}[q_i(t) - q_j(t) - \delta_{ij}(t)] = \lim_{t\to\infty}[\xi_i(t) - \xi_j(t) - \delta_{ij}(t)] = 0$, which confirms (O3) and (O1) are satisfied. ■

Proposition 1 shows that if $\mathcal{A}+\mathcal{A}_{\mathrm{d}}$ is nonsingular, ϕ is linear, and the gains are selected such that $b_i = \kappa a_i$ and $\beta_{ij} = \kappa\alpha_{ij}$, where κ satisfies (24), then A is asymptotically stable and (O1)–(O4) are satisfied. The lower bound (24) on κ depends on D; however, Lemma 3 provides a construction of D using $\mathcal{A}+\mathcal{A}_{\mathrm{d}}$. Thus, the control gains can be designed by: i) selecting α_{ij} and a_i; ii) constructing D using Lemma 3; iii) selecting κ to satisfy (24); and iv) selecting $\beta_{ij} = \kappa\alpha_{ij}$ and $b_i = \kappa a_i$.

Proposition 1 requires that b_i and β_{ij} are proportional to a_i and α_{ij}, and that the proportional constant κ satisfies (24). In Example 6, the velocity gains are proportional to the position gains. However, $\kappa = 0.3$ does not satisfy (24) because $\sqrt{\frac{2}{\phi_0}\lambda_{\max}(D^{1/2}Q^{-1}D^{1/2})} = 2.0945$.

The following result extends Proposition 1 to address the case where the communication is directed and ϕ is nonlinear. This result provides sufficient conditions such that the origin is a locally asymptotically stable equilibrium of (7)–(9), and (O1)–(O4) are satisfied locally.

Theorem 2. Consider the closed-loop dynamics (7)–(9), which consists of (1)–(5). Assume that ϕ is such that $\frac{\partial\phi(x)}{\partial x}|_{x=0} = \phi_0 I_m$, where $\phi_0 > 0$, and assume that $\mathcal{A}+\mathcal{A}_{\mathrm{d}}$ is nonsingular. Let $\kappa > 0$ satisfy (24), where $D \in \mathbb{R}^{n\times n}$

and $Q \in \mathbb{R}^{n\times n}$ are the positive-definite matrices given by Lemma 3. For all $i \in \mathcal{I}$, let $b_i = \kappa a_i$, and for all $(i,j) \in \mathcal{P}$, let $\beta_{ij} = \kappa\alpha_{ij}$. Then, the origin is a locally asymptotically stable equilibrium of (7)–(9). Furthermore, there exists an open set $\mathcal{D} \subset \mathbb{R}^{mn} \times \mathbb{R}^{mn}$ that contains the origin such that for all $(\xi(0), \rho(0)) \in \mathcal{D}$, (O1)–(O4) are satisfied.

Proof: Linearizing (7)–(9) about the origin yields (22) and (23), where Proposition 1 implies that (23) is asymptotically stable. Thus, Lyapunov's indirect method implies that the origin is a locally asymptotically stable equilibrium, and it follows that there exists an open set $\mathcal{D}$ such that for all $(\xi(0), \rho(0)) \in \mathcal{D}$, $\lim_{t\to\infty} \xi(t) = 0$ and $\lim_{t\to\infty} \rho(t) = 0$, which implies that (O1)–(O4) are satisfied. ■

Theorem 2 shows that if $\mathcal{A} + \mathcal{A}_\mathrm{d}$ is nonsingular and the gains satisfy $b_i = \kappa a_i$ and $\beta_{ij} = \kappa\alpha_{ij}$, where κ satisfies (24), then (O1)–(O4) are satisfied locally. Numerical testing suggests that these conditions are sufficient to satisfy (O1)–(O4) globally; however, a proof of this result is open. The following numerical example demonstrates Theorem 2.

Simulation 2. Let $n = 4$ and $m = 3$, and let ϕ be given by Example 4, which implies that $\phi_0 = 1$. Let $\mathcal{N}_1 = \{2\}$, $\mathcal{N}_2 = \{3\}$, $\mathcal{N}_3 = \{4\}$, and $\mathcal{N}_4 = \{1\}$, which represents a directed cyclic feedback structure. For all $j \in \mathcal{N}_i$, let $\alpha_{ij} = 0.5$, and let $a_1 = 0.8$ and $a_2 = a_3 = a_4 = 0$. Let $\kappa = 4$, which satisfies (24) because $\sqrt{2\lambda_{\max}(D^{1/2}Q^{-1}D^{1/2})} = 3.119$. Thus, we let $\beta_{ij} = \kappa\alpha_{ij} = 2.0$, $b_1 = \kappa a_1 = 3.2$, and $b_2 = b_3 = b_4 = 0$, which implies that only the first agent has a measurement of its position and velocity relative to the leader.

Let $R(t) \in \mathrm{SO}(3)$ satisfy $\dot{R}(t) = R(t)\Omega$, where $R(0) = I_3$, $\Omega = [\omega]_\times$, and $\omega = \begin{bmatrix} 2\pi/5 & 0 & -\pi/15 \end{bmatrix}^\mathrm{T}$ rad/s. Define $d_1 \triangleq e_1$ m, $d_2 \triangleq -e_2$ m, $d_3 \triangleq -e_1$ m, and $d_4 \triangleq e_2$ m, which are the desired positions of each agent relative to the leader resolved in the frame defined by R^T. Thus, the desired time-varying positions are $\delta_i = Rd_i$. The leader's position is given by (21).

Figure 4 shows the three-dimensional agent trajectories q_i and the desired trajectories $q_\mathrm{g} + \delta_i$ from $t_1 = 15$ s to $t_2 = 30$ s. At $t_1 = 15$ s the agents are not in the desired time-varying formation; however, by $t_2 = 30$ s, the agents reach and maintain the desired time-varying formation. Figures 5 and 6 show that $\lim_{t\to\infty} \xi_i(t) = 0$ and $\lim_{t\to\infty} \rho_i(t) = 0$, which implies that (O1)–(O4) are satisfied. △

VII. Formation Control with Collision Avoidance

In this section, we extend the formation control (5) to include collision-avoidance terms that prevent the ith agent from colliding with agents in its neighbor set $\mathcal{N}_i$, or colliding with the leader if the ith agent has a measurement of its position relative to the leader. Define $\mathcal{I}_a \triangleq \{i \in \mathcal{I} \colon a_i > 0\}$, which is the set of agents that have a measurement of their position relative to the leader. Define the collision radius $r_\mathrm{c} > 0$. Then, the objective is to design a control u_i such that (O1)–(O4) are achieved, and:

(O5) For all $(i,j) \in \mathcal{I}\times\mathcal{N}_i$ and all $t \geq 0$, $\|q_i(t) - q_j(t)\| > r_\mathrm{c}$.
(O6) For all $i \in \mathcal{I}_a$ and all $t \geq 0$, $\|q_i(t) - q_\mathrm{g}(t)\| > r_\mathrm{c}$.

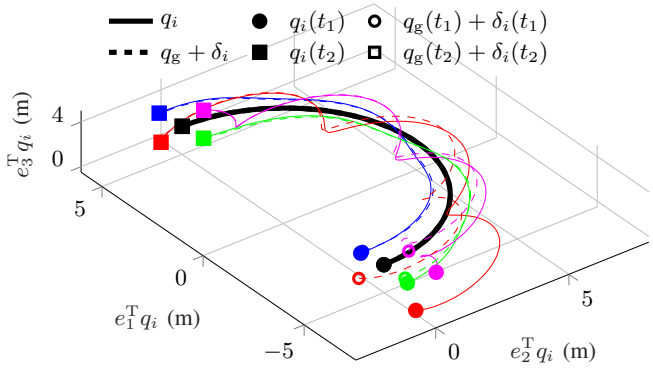

Fig. 4. Three-dimensional agent position q_i and desired time-varying position $q_\mathrm{g} + \delta_i$ from $t_1 = 15$ s to $t_2 = 30$ s for agents $i = 1$ (blue), $i = 2$ (red), $i = 3$ (green), and $i = 4$ (magenta). The leader trajectory q_g is shown in black. By $t_2 = 30$ s, the agents achieve the desired time-varying formation.

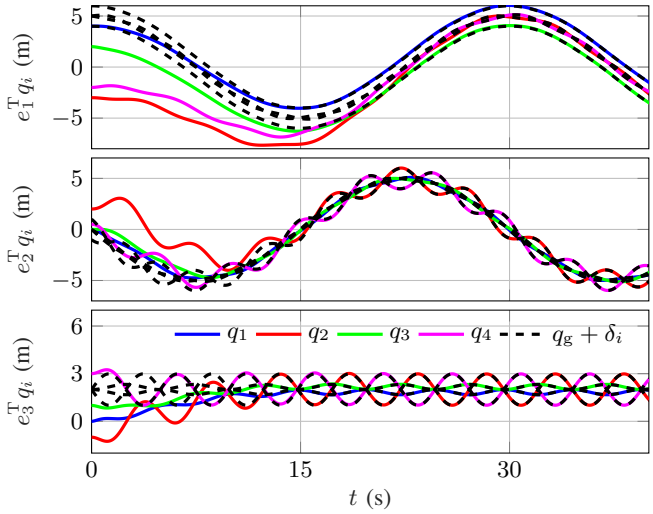

Fig. 5. Position q_i and desired position $q_\mathrm{g} + \delta_i$. (O1) and (O3) are satisfied.

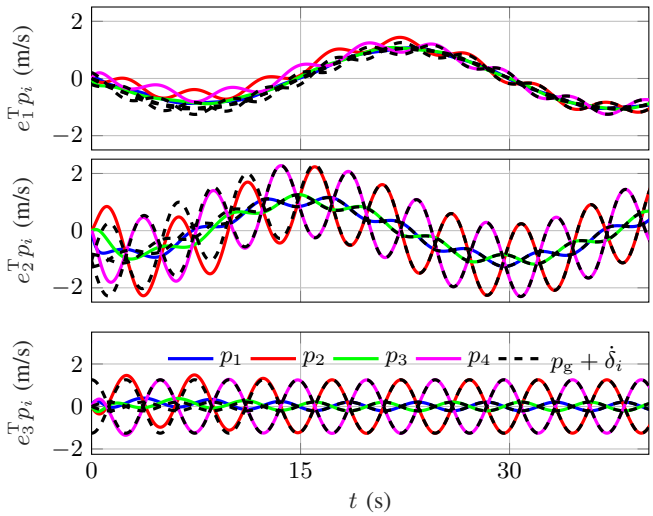

Fig. 6. Position p_i and desired position $p_\mathrm{g} + \dot{\delta}_i$. (O2) and (O4) are satisfied.

In the case of all-to-all communication (i.e., $\mathcal{N}_i = \mathcal{I}$), objective (O5) implies that there are no collisions among

any agents. We note that (O6) may not be important for applications where the leader is not a physical agent.

In order to achieve (O1) and (O3) as well as (O5) and (O6), it is necessary to assume that the desired positions δ_i and δ_{ij} have magnitude greater than the collision radius r_{c}. Thus, we assume that there exists $d > r_{\mathrm{c}}$ such that

$$\inf_{t\geq 0} \|\delta_i(t)\| > d, \qquad \inf_{t\geq 0} \|\delta_{ij}(t)\| > d. \tag{27}$$

A. Formation Control Algorithm with Collision Avoidance

To develop the collision-avoidance function, let $h \in (0,1)$, and consider $\mu_h : [0,\infty) \to [0,1]$ defined by

$$\mu_h(\zeta) \triangleq \begin{cases} 1, & \text{if } \zeta \in [0,h), \\ \frac{1}{2} + \frac{1}{2}\cos \pi \frac{\zeta - h}{1-h}, & \text{if } \zeta \in [h,1], \\ 0, & \text{if } \zeta \in (1,\infty), \end{cases} \tag{28}$$

which decreases from 1 to 0 as ζ increases from 0 to 1. Next, consider $\psi : [0,\infty) \to [-d^2/\sqrt{1+d^4}, 0]$ defined by

$$\psi(\zeta) \triangleq \mu_h\left(\frac{\zeta}{d^2}\right)\left[\frac{\zeta - d^2}{\sqrt{1+(\zeta-d^2)^2}}\right], \tag{29}$$

and note that if $\zeta \geq d^2$, then $\psi(\zeta) = 0$; otherwise, $\psi(\zeta) < 0$. In addition, note that ψ is continuously differentiable on $[0,\infty)$. Consider the potential function $\Psi : [0,\infty) \to [0,\infty)$ defined by

$$\Psi(\zeta) \triangleq \frac{1}{2}\int_{d^2}^{\zeta} \psi(s)\,\mathrm{d}s, \tag{30}$$

and note that if $\zeta \geq d^2$, then $\Psi(\zeta) = 0$; otherwise, $\Psi(\zeta) > 0$. Finally, consider the collision-avoidance function $\sigma\colon \mathbb{R}^m \to \mathbb{R}^m$ defined by

$$\sigma(x) \triangleq \left[\frac{\partial \Psi\big(\|x\|^2\big)}{\partial x}\right]^{\mathrm{T}} = \psi\big(\|x\|^2\big)x. \tag{31}$$

To achieve objectives (O1)–(O6), we consider the control

$$\begin{aligned} u_i \triangleq\ & u_{\mathrm{g}} + \ddot{\delta}_i + a_i\phi(q_{\mathrm{g}} - q_i + \delta_i) + b_i\phi\Big(p_{\mathrm{g}} - p_i + \dot{\delta}_i\Big) \\ & + \sum_{j\in\mathcal{N}_i}\Big[\alpha_{ij}\phi(q_j - q_i + \delta_{ij}) + \beta_{ij}\phi\Big(p_j - p_i + \dot{\delta}_{ij}\Big)\Big] \\ & + g_i\sigma(q_{\mathrm{g}} - q_i) + \sum_{j\in\mathcal{N}_i}\gamma_{ij}\sigma(q_j - q_i), \end{aligned} \tag{32}$$

where $a_i, b_i, g_i \geq 0$; for all $j \in \mathcal{N}_i$, $\alpha_{ij}, \beta_{ij}, \gamma_{ij} > 0$; and for all $j \notin \mathcal{N}_i$, $\alpha_{ij} = \beta_{ij} = \gamma_{ij} = 0$.

The control (32) is similar to the control (5) except (32) includes the extra terms $\sigma(q_{\mathrm{g}} - q_i)$ and $\sigma(q_j - q_i)$ that act, if necessary, to repel agent i from the leader and agent j, respectively. Specifically, if agents i and j are close to one another and in danger of colliding (i.e., $\|q_j - q_i\| < d$), then it follows from (29) that $\psi(\|q_j - q_i\|^2) < 0$. In this case, (31) implies that $\sigma(q_j - q_i)$ acts to repel agent i directly away from agent j. In contrast, if agents i and j are sufficiently far apart (i.e., $\|q_j - q_i\| > d$), then (28), (29), and (31) imply that $\sigma(q_j - q_i) = 0$ and thus does not contribute to the control (32). Similar observations hold for the term $\sigma(q_{\mathrm{g}} - q_i)$, which repels agent i from the leader. Also, note that σ is bounded. Thus, if $\ddot{u}_{\mathrm{g}}$ and $\ddot{\delta}_i$ are bounded and ϕ is selected as a bounded function (e.g., Examples 2–4), then the control (32) is bounded.

Differentiating (6) and using (1)–(4) and (32) yields the closed-loop dynamics (7) and (8), where

$$\begin{aligned} \hat{u}_i \triangleq\ & -a_i\phi\left(\xi_i\right) - b_i\phi\left(\rho_i\right) - g_i\sigma(\xi_i + \delta_i) + \sum_{j\in\mathcal{N}_i}\Big[\alpha_{ij}\phi(\xi_j - \xi_i) \\ & + \beta_{ij}\phi\left(\rho_j - \rho_i\right) + \gamma_{ij}\sigma(\xi_j - \xi_i - \delta_{ij})\Big]. \end{aligned} \tag{33}$$

B. Analysis with Collision Avoidance

We now analyze the closed-loop dynamics (7), (8), and (33) under the assumption that δ_i are constant. Thus, for the remainder of this section, we assume that $\dot{\delta}_i = 0$. Next, define

$$c_i \triangleq \max_{\|x+\delta_i\|\leq d} \frac{-x^{\mathrm{T}}\sigma(x+\delta_i)}{x^{\mathrm{T}}\phi(x)}, \tag{34}$$

$$c_{ij} \triangleq \max_{\|x+\delta_{ij}\|\leq d} \frac{-x^{\mathrm{T}}\sigma(x+\delta_{ij})}{x^{\mathrm{T}}\phi(x)}, \tag{35}$$

and note that it follows from (C3) and (27)–(31) that $c_i > 0$ and $c_{ij} > 0$. The following result is needed to analyze stability. The proof is in Appendix A.

Lemma 4. Let $\varepsilon_i, \varepsilon_{ij} \in [0,1)$. Then, for all $x \in \mathbb{R}^m \setminus \{0\}$,

$$x^{\mathrm{T}}\phi(x) + \frac{\varepsilon_i}{c_i}x^{\mathrm{T}}\sigma(x+\delta_i) > 0, \tag{36}$$

$$x^{\mathrm{T}}\phi(x) + \frac{\varepsilon_{ij}}{c_{ij}}x^{\mathrm{T}}\sigma(x+\delta_{ij}) > 0. \tag{37}$$

Next, consider the Lyapunov-like function $V : \mathbb{R}^{mn} \times \mathbb{R}^{mn} \to [0,\infty)$ defined by

$$\begin{aligned} V(\xi,\rho) \triangleq\ & \sum_{i\in\mathcal{I}}\Bigg[a_i\Phi(\xi_i) + g_i\Psi(\|\xi_i + \delta_i\|^2) + \frac{1}{2}\rho_i^{\mathrm{T}}\rho_i \\ & + \sum_{j\in\mathcal{N}_i}\left[\frac{\alpha_{ij}}{2}\Phi(\xi_i - \xi_j) + \frac{\gamma_{ij}}{2}\Psi(\|\xi_i - \xi_j + \delta_{ij}\|^2)\right]\Bigg]. \end{aligned} \tag{38}$$

Since Φ is positive definite and Ψ is nonnegative, it follows from (38) that V is nonnegative.

The following theorem is the main result that addresses the control (32) with an undirected communication structure. This result shows that if $\mathcal{G}$ is quasi-strongly connected and at least one agent has a measurement of its position and velocity relative to the leader, then the origin is a globally asymptotically stable equilibrium of (7), (8), and (33), and (O1)–(O4) are satisfied. This result also describes initial conditions for which there are no collisions. Define $\mathcal{S} \triangleq \{x \in \mathbb{R}^m : \|x\| = r_{\mathrm{c}}\}$.

Theorem 3. Consider the closed-loop dynamics (7), (8), and (33), which consists of (1)–(4) and (28)–(32). Assume that $\mathcal{G} = (\mathcal{I}, \mathcal{E})$ is quasi-strongly connected, and assume that for all $i \in \mathcal{I}$, $\delta_i = 0$. For all $i \in \mathcal{I}$, let $g_i \in [0, a_i/\bar{c}_i]$, where $\bar{c}_i > c_i$ and c_i is given by (34). For all $(i,j) \in \mathcal{P}$, let $\alpha_{ij} = \alpha_{ji}$, $\beta_{ij} = \beta_{ji}$, and $\gamma_{ij} = \gamma_{ji} \in [0, \alpha_{ij}/\bar{c}_{ij}]$, where $\bar{c}_{ij} > c_{ij}$ and c_{ij} is given by (35). Then, the following statements hold:

i) Assume that for all $i \in \mathcal{I}$, $a_i = 0$ and $b_i = 0$. Then, for all $(\xi(0), \rho(0)) \in \mathbb{R}^{2mn}$, (O1) and (O2) are satisfied.

ii) Assume that there exists $\ell \in \mathcal{I}$ such that $b_\ell > 0$. Then, for all $(\xi(0), \rho(0)) \in \mathbb{R}^{2mn}$, (O1), (O2), and (O4) are satisfied.

iii) Assume that there exist $\ell_1, \ell_2 \in \mathcal{I}$ such that $a_{\ell_1} > 0$ and $b_{\ell_2} > 0$. Then, the origin is a globally asymptotically stable equilibrium of (7)–(9), and for all $(\xi(0), \rho(0)) \in \mathbb{R}^{2mn}$, (O1)–(O4) are satisfied.

iv) Assume that $(\xi(0), \rho(0)) \in \mathbb{R}^{2mn}$ satisfy

$$V(\xi(0), \rho(0)) < \min_{(i,j)\in\mathcal{I}\times\mathcal{N}_i} \Big[\gamma_{ij}\Psi(r_{\mathrm{c}}^2) + \min_{x\in\mathcal{S}} \alpha_{ij}\Phi(x-\delta_{ij})\Big].$$

Then, (O5) is satisfied.

v) Assume that $(\xi(0), \rho(0)) \in \mathbb{R}^{2mn}$ satisfy

$$V(\xi(0), \rho(0)) < \min_{i\in\mathcal{I}_a} \Big[g_i\Psi(r_{\mathrm{c}}^2) + \min_{x\in\mathcal{S}} a_i\Phi(x-\delta_i)\Big].$$

Then, (O6) is satisfied.

Proof: Note that for all $x \in \mathbb{R}^m$, $\sigma(x) = -\sigma(-x)$, which implies that Lemma 1 holds with ϕ replaced by σ. Thus, using the same process used from (10) to (11) in the proof of Theorem 1 implies that

$$\dot{V}(\xi,\rho) \triangleq \sum_{i\in\mathcal{I}} \left[\frac{\partial V}{\partial \xi_i}\dot{\xi}_i + \frac{\partial V}{\partial \rho_i}\dot{\rho}_i\right] = -\sum_{i\in\mathcal{I}} \Big[b_i\rho_i^{\mathrm{T}}\phi(\rho_i) + \sum_{j\in\mathcal{N}_i} \frac{\beta_{ij}}{2}(\rho_i-\rho_j)^{\mathrm{T}}\phi(\rho_i-\rho_j)\Big], \tag{39}$$

which is nonpositive. Thus, V is bounded, and it follows from (38) that ρ_i is bounded; $\xi_i - \xi_j$ is bounded; and for all $i \in \mathcal{I}_a$, ξ_i is bounded. Next, using the same arguments as in the proof of Theorem 1, it follows that $\lim_{t\to\infty}[\rho_i(t) - \rho_j(t)] = 0$; for all $i \in \mathcal{I}_b \triangleq \{i \in \mathcal{I}\colon b_i > 0\}$, $\lim_{t\to\infty} \rho_i(t) = 0$; and (O2) is satisfied.

Note that since ϕ and σ are continuously differentiable, using the same arguments used in the proof of Theorem 1, it follows that $\dot{\rho}_i$ is uniformly continuous.

Furthermore, using (8) and (33), and the same process used from (13) to (14) in the proof of Theorem 1 implies that

$$-\sum_{i\in\mathcal{I}} \xi_i^{\mathrm{T}}\dot{\rho}_i = \sum_{i\in\mathcal{I}_a} a_i\Big[\xi_i^{\mathrm{T}}\phi(\xi_i) + \frac{\varepsilon_i}{c_i}\xi_i^{\mathrm{T}}\sigma(\xi_i+\delta_i)\Big] + \sum_{i\in\mathcal{I}_b} b_i\xi_i^{\mathrm{T}}\phi(\rho_i) + \sum_{(i,j)\in\mathcal{I}\times\mathcal{N}_i} \Bigg(\frac{\beta_{ij}}{2}(\xi_i-\xi_j)^{\mathrm{T}} \times \phi(\rho_i-\rho_j) + \frac{\alpha_{ij}}{2}\Big[(\xi_i-\xi_j)^{\mathrm{T}}\phi(\xi_i-\xi_j) + \frac{\varepsilon_{ij}}{c_{ij}}(\xi_i-\xi_j)^{\mathrm{T}}\sigma(\xi_i-\xi_j+\delta_{ij})\Big]\Bigg), \tag{40}$$

where $\varepsilon_i \triangleq g_i c_i/a_i \in [0,1)$ and $\varepsilon_{ij} \triangleq \gamma_{ij}c_{ij}/\alpha_{ij} \in [0,1)$.

To show iii), assume that there exist $\ell_1, \ell_2 \in \mathcal{I}$ such that $a_{\ell_1} > 0$ and $b_{\ell_2} > 0$. Since $\lim_{t\to\infty} \rho_{\ell_2}(t) = 0$, and $\lim_{t\to\infty}[\rho_i(t) - \rho_j(t)] = 0$, it follows that $\lim_{t\to\infty} \rho_i(t) = 0$, which confirms (O4). Since $\lim_{t\to\infty} \int_0^t \dot{\rho}_i(\tau)\,\mathrm{d}\tau = \lim_{t\to\infty} \rho_i(t)$ exists and $\dot{\rho}_i$ is uniformly continuous, it follows from Barbalat's Lemma [49, Lemma 8.2] that $\lim_{t\to\infty} \dot{\rho}_i(t) = 0$. Since ξ_{ℓ_1} is bounded and $\xi_i - \xi_j$ is bounded, it follows that ξ_i is bounded. Thus, $\lim_{t\to\infty} \sum_{i\in\mathcal{I}} \xi_i^{\mathrm{T}}(t)\dot{\rho}_i(t) = 0$. Since, in addition, $\lim_{t\to\infty} \rho_i(t) = 0$, taking the limit as $t \to \infty$ of (40) implies

$$0 = \lim_{t\to\infty} \Bigg(\sum_{i\in\mathcal{I}_a} a_i\Big[\xi_i^{\mathrm{T}}(t)\phi(\xi_i(t)) + \frac{\varepsilon_i}{c_i}\xi_i^{\mathrm{T}}(t)\sigma(\xi_i(t)+\delta_i)\Big] + \sum_{(i,j)\in\mathcal{I}\times\mathcal{N}_i} \frac{\alpha_{ij}}{2}\Big[(\xi_i(t)-\xi_j(t))^{\mathrm{T}}\phi(\xi_i(t)-\xi_j(t)) + \frac{\varepsilon_{ij}}{c_{ij}}(\xi_i(t)-\xi_j(t))^{\mathrm{T}}\sigma(\xi_i(t)-\xi_j(t)+\delta_{ij})\Big]\Bigg), \tag{41}$$

where it follows from Lemma 4 that each term inside of square brackets in (41) is nonnegative, and thus, converge to zero. Thus, $\lim_{t\to\infty} \xi_{\ell_1}(t) = 0$ and for all $(i,j) \in \mathcal{I} \times \mathcal{N}_i$, $\lim_{t\to\infty}[\xi_i(t) - \xi_j(t)] = 0$. Since, in addition, $\mathcal{G}$ is quasi-strongly connected, it follows that $\lim_{t\to\infty}[\xi_i(t) - \xi_j(t)] = 0$, which confirms (O1). Since, in addition, $\lim_{t\to\infty} \xi_{\ell_1}(t) = 0$, it follows that $\lim_{t\to\infty} \xi_i(t) = 0$, which confirms (O3). Thus, (O1)–(O4) are satisfied. Since $a_{\ell_1} > 0$, (38) implies that V is positive definite, which implies that the origin is a Lyapunov stable equilibrium of (7), (8), and (33) because $\dot{V}$ is nonpositive. Since, in addition, $\lim_{t\to\infty} \xi_i(t) = 0$ and $\lim_{t\to\infty} \rho_i(t) = 0$, it follows that the origin is a globally asymptotically stable equilibrium, which verifies iii).

To show i) and ii), assume without loss of generality that $a_i = 0$, which implies that $g_i = 0$. Consider $W : \mathbb{R}^{mn} \times \mathbb{R}^{mn} \to \mathbb{R}$ defined by (16). Since $a_i = g_i = 0$ and for all $j \notin \mathcal{N}_i$, $\alpha_{ij} = 0$, $\beta_{ij} = 0$, and $\gamma_{ij} = 0$, it follows from (8) and (33) that

$$\sum_{i\in\mathcal{I}} \dot{\rho}_i = -\sum_{i\in\mathcal{I}_b} b_i\phi(\rho_i) + \sum_{(i,l)\in\mathcal{P}} \Big[\alpha_{il}\phi(\xi_l-\xi_i) + \beta_{il}\phi(\rho_l-\rho_i) + \gamma_{il}\sigma(\xi_l-\xi_i-\delta_{il})\Big],$$

and since $\alpha_{ij} = \alpha_{ji}$, $\beta_{ij} = \beta_{ji}$, and $\gamma_{ij} = \gamma_{ji}$, it follows from (C2) and the fact that $\sigma(x) = -\sigma(-x)$ that

$$\sum_{i\in\mathcal{I}} \dot{\rho}_i = -\sum_{i\in\mathcal{I}_b} b_i\phi(\rho_i). \tag{42}$$

Substituting (40) and (42) into (16) yields

$$W(\xi,\rho) = \sum_{(i,j)\in\mathcal{I}_b\times\mathcal{I}} b_i(\xi_i-\xi_j)^{\mathrm{T}}\phi(\rho_i) + n\sum_{(i,j)\in\mathcal{I}\times\mathcal{N}_i} (\xi_i-\xi_j)^{\mathrm{T}} \times \Bigg(\frac{\beta_{ij}}{2}\phi(\rho_i-\rho_j) + \frac{\alpha_{ij}}{2}\Big[\phi(\xi_i-\xi_j) + \frac{\varepsilon_{ij}}{c_{ij}}\sigma(\xi_i-\xi_j+\delta_{ij})\Big]\Bigg). \tag{43}$$

Since $\lim_{t\to\infty} \int_0^t \dot{\rho}_i(\tau) - \dot{\rho}_j(\tau)\,\mathrm{d}\tau = \lim_{t\to\infty}[\rho_i(t) - \rho_j(t)]$ exists and $\dot{\rho}_i - \dot{\rho}_j$ is uniformly continuous, it follows from Barbalat's Lemma that $\lim_{t\to\infty}[\dot{\rho}_i(t) - \dot{\rho}_j(t)] = 0$. Since, in addition, $\xi_i - \xi_j$ is bounded, it follows from (16) that $\lim_{t\to\infty} W(\xi(t), \rho(t)) = 0$. Since, in addition, $\lim_{t\to\infty}[\rho_i(t) - \rho_j(t)] = 0$ and for all $i \in \mathcal{I}_b$, $\lim_{t\to\infty} \rho_i(t) = 0$, taking the limit as $t \to \infty$ of (43) implies that

$$0 = \lim_{t\to\infty} \sum_{(i,j)\in\mathcal{I}\times\mathcal{N}_i} \frac{\alpha_{ij}}{2}\Big[(\xi_i(t)-\xi_j(t))^{\mathrm{T}}\phi(\xi_i(t)-\xi_j(t))$$

$$+\frac{\varepsilon_{ij}}{c_{ij}}(\xi_i(t)-\xi_j(t))^{\mathrm{T}}\sigma(\xi_i(t)-\xi_j(t)+\delta_{ij})\Big], \qquad (44)$$

where it follows from Lemma 4 that each term in the summation is nonnegative, and thus, converge to zero. Thus, for all $(i,j)\in\mathcal{I}\times\mathcal{N}_i$, $\lim_{t\to\infty}[\xi_i(t)-\xi_j(t)]=0$. Since, in addition, $\mathcal{G}$ is quasi-strongly connected, it follows that $\lim_{t\to\infty}[\xi_i(t)-\xi_j(t)]=0$, which confirms (O1), and thus, verifies i).

To show ii), assume that there exists $\ell\in\mathcal{I}$ such that $b_\ell>0$. Since $\lim_{t\to\infty}\rho_\ell(t)=0$, and $\lim_{t\to\infty}[\rho_i(t)-\rho_j(t)]=0$, it follows that $\lim_{t\to\infty}\rho_i(t)=0$, which confirms (O4), and thus, verifies ii).

To show iv), assume that

$$V(\xi(0),\rho(0))<\min_{(i,j)\in\mathcal{I}\times\mathcal{N}_i}[\gamma_{ij}\Psi(r_{\mathrm{c}}^2)+\min_{x\in\mathcal{S}}\alpha_{ij}\Phi(x-\delta_{ij})].$$

Let $(k,l)\in\mathcal{I}\times\mathcal{N}_k$, and (38) implies that $\gamma_{kl}\Psi(\|q_k-q_l\|^2)+\alpha_{kl}\Phi(q_k-q_l-\delta_{kl})\leq V(\xi,\rho)$. Since, in addition, $\dot V(\xi,\rho)\leq 0$, it follows that for all $t\geq 0$, $\gamma_{kl}\Psi(\|q_k(t)-q_l(t)\|^2)+\alpha_{kl}\Phi(q_k(t)-q_l(t)-\delta_{kl})\leq V(\xi(t),\rho(t))\leq V(\xi(0),\rho(0))<\gamma_{kl}\Psi(r_{\mathrm{c}}^2)+\min_{x\in\mathcal{S}}\alpha_{kl}\Phi(x-\delta_{kl})$. Thus, for all $t\geq 0$, $\|q_k(t)-q_l(t)\|>r_{\mathrm{c}}$, which confirms iv).

Finally, v) is confirmed using arguments similar to those used to show iv). ■

Note that i)–iii) of Theorem 3 are identical to the results in Theorem 1. Thus, the collision-avoidance terms in (32), which are not in (5), do not negatively impact accomplishing the formation objectives (O1)–(O4). Furthermore, iv) provides a set of initial conditions for which there are no collisions between agents and their neighbors, and v) provides a set of initial conditions for which there are no collisions between the leader and agents who have a measurement of their position relative to the leader. Analysis of (7), (8), and (33) with time-varying δ_i is an open problem.

The following result extends Theorem 2 to address the control (32) in the case where the communication is directed. The result provides sufficient conditions such that the origin is a locally asymptotically stable equilibrium of (7), (8), and (33), and (O1)–(O6) are satisfied locally. The next theorem is a consequence of Proposition 1 and Lyapunov's indirect method. The proof is similar to that of Theorem 2 and is omitted for brevity.

Theorem 4. Consider the closed-loop dynamics (7), (8), and (33), which consists of (1)–(4) and (28)–(32). Assume that ϕ is such that $\frac{\partial\phi(x)}{\partial x}|_{x=0}=\phi_0 I_m$, where $\phi_0>0$. Assume that $\mathcal{A}+\mathcal{A}_{\mathrm{d}}$ is nonsingular, and assume that for all $i\in\mathcal{I}$, $\dot\delta_i=0$. Let $\kappa>0$ satisfy (24), where $D\in\mathbb{R}^{n\times n}$ and $Q\in\mathbb{R}^{n\times n}$ are the positive-definite matrices given by Lemma 3. For all $i\in\mathcal{I}$, let $b_i=\kappa a_i$, and let $g_i>0$ if and only if $a_i>0$. For all $(i,j)\in\mathcal{P}$, let $\beta_{ij}=\kappa\alpha_{ij}$, and let $\gamma_{ij}>0$ if and only if $\alpha_{ij}>0$. Then, the origin is a locally asymptotically stable equilibrium of (7), (8), and (33). Furthermore, there exists an open set $\mathcal{D}\subset\mathbb{R}^{mn}\times\mathbb{R}^{mn}$ that contains the origin such that for all $(\xi(0),\rho(0))\in\mathcal{D}$, (O1)–(O6) are satisfied.

The following numerical example demonstrates the control (32). The initial conditions are selected such that Theorem 3 guarantees that (32) prevents collisions. This example also demonstrates that the control (5), which does not include collision-avoidance terms but is otherwise identical to (32), results in a collision, whereas the control (32) does not.

Simulation 3. Let $n=2$ and $m=2$, and let ϕ be given by Example 2 with $\nu=1$. Let $\mathcal{N}_1=\{2\}$, $\mathcal{N}_2=\{1\}$, and let $\alpha_{12}=\alpha_{21}=6$, $\beta_{12}=\beta_{21}=0.5$, $a_1=a_2=0$, and $b_1=b_2=0$. Thus, there is no leader.

The collision radius is $r_{\mathrm{c}}=0.3$ m, and we let $d=2$ m and $h=0.9$. The desired interagent position is $\delta_{12}=[-3\quad 0]^{\mathrm{T}}$ m. We approximate c_{12} given by (35) using a grid search over $\{x\in\mathbb{R}^2:||x+\delta_{12}||<d\}$, which yields $c_{12}=c_{21}=1.347$. Thus, we let $g_{12}=g_{21}=4.286$ and $g_1=g_2=0$, which satisfy that assumptions of Theorem 3.

Since Φ is given by Example 2, it follows the assumption in iv) of Theorem 3 is satisfied if

$$V(\xi(0),\rho(0))<\gamma_{12}\Psi(r_{\mathrm{c}}^2)+\alpha_{12}\Phi\left(\frac{\|\delta_{12}\|-r_{\mathrm{c}}}{\|\delta_{12}\|}\delta_{12}\right)=17.62.$$

Let $q_1(0)=[-3.8\quad 0.1]^{\mathrm{T}}$ m, $q_2(0)=[3\quad 0]^{\mathrm{T}}$ m, and $p_1(0)=p_2(0)=[0\quad 0]$ m/s, which yields $V(\xi(0),\rho(0))=17.58<17.62$. Thus, Theorem 3 guarantees no collisions.

Figures 7 shows that (O1) is satisfied using either the control (32) that includes collision avoidance, or the control (5) that does not include the collision-avoidance terms but is otherwise identical to (32). Similarly, both controls satisfy (O2). However, Figure 8 demonstrates that (32) prevents collision, whereas using (5) results in a collision. △

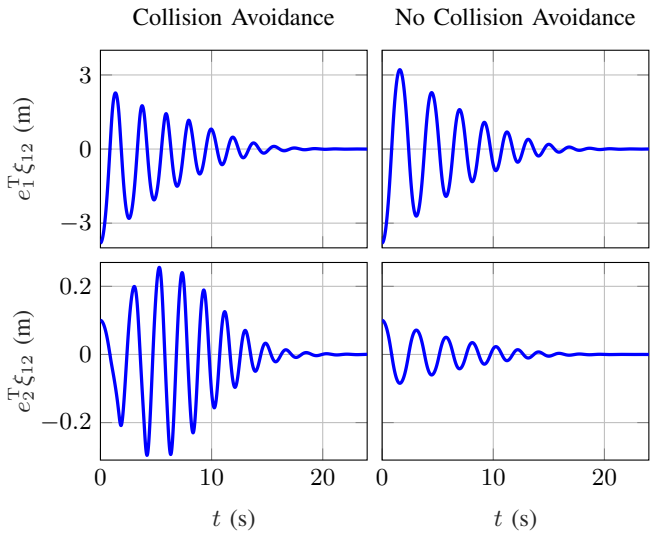

Fig. 7. Position error $\xi_{12}\triangleq\xi_1-\xi_2$. Objective (O1) is satisifed.

VIII. Indoor Rotorcraft Experiments

This section presents results from indoor experiments using three 3D-Robotics Solo quadcopters (see Figure 9) and an OptiTrack motion-capture system. We attach 4 retro-reflective markers (OptiTrack's 15.9 mm markers with M4 base) to each quadcopter in an asymmetric-and-unique pattern, which allows the motion-capture system to track each quadcopter's position and attitude based on marker placement.

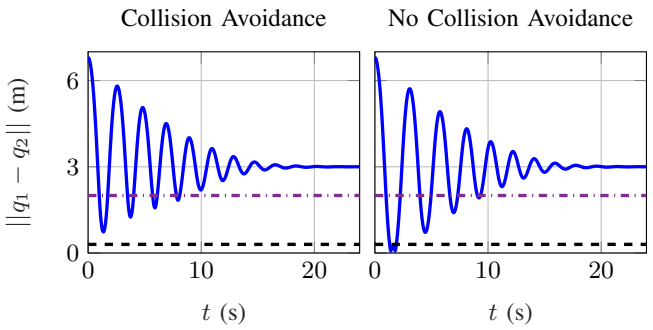

Fig. 8. Using the control (32), $\|q_1 - q_2\|$ is bounded above the collision radius r_c (dashed line). In contrast, using the control (5) (i.e., no collision avoidance), $\|q_1 - q_2\|$ drops below r_c, which results in a collision. Note that when $\|q_1 - q_2\|$ is below d (dashed-dotted line), the collision-avoidance terms in (32) are nonzero.

Fig. 9. The photo on the left shows the three 3DR Solo quadcopters used in the indoor and outdoor experiments. The photo on the right shows a close-up view of one quadcopter with its onboard Raspberry Pi 3B+ and custom hardware in the accessory bay.

We use 6 OptiTrack Prime 13 cameras and 6 OptiTrack Prime 13W cameras, which emit and receive infrared light to track objects. The cameras are mounted to walls 3.3 m off the ground, and the tracking volume is 12 m by 6 m by 3.3 m.

A desktop computer runs Motive:Tracker 1.0 software, which can track each quadcopter's position resolved in a fixed inertial frame (i.e., the motion-capture frame) and each quadcopter's attitude relative to this inertial frame. We estimate velocity using a backward difference and low-pass filter. The desktop computer sends this feedback data to each quadcopter using an ad hoc wireless network.

Each quadcopter is attitude stabilized using the Arducopter 3.3 inner-loop controller in 'stabilize' mode, which is implemented on the quadcopter's onboard Pixhawk Cube 2.0 flight controller. We tune the sensitivity of the pitch and roll stick-commands, but do not alter this inner-loop controller. The inner-loop controller accepts pulse-width-modulation (PWM) pitch, roll, and throttle commands, which are prescribed using the 'vehicle.channels.overrides' command in the dronekit API.

The PWM pitch, roll, and throttle commands are sent to the Pixhawk's inner-loop flight controller from an onboard Raspberry Pi 3B+ at 10 Hz through the serial2 port in the quadcopter's accessory bay; this custom hardware configuration is shown in Figure 9. The Pi obtains feedback measurements of the quadcopter's pitch and roll from the Pixhawk. The Pi is connected to the ad hoc wireless network and receives the motion-capture estimates of the agents' positions, velocities, and yaw angles, as well as the required information regarding the time-varying formation and the leader (if applicable).

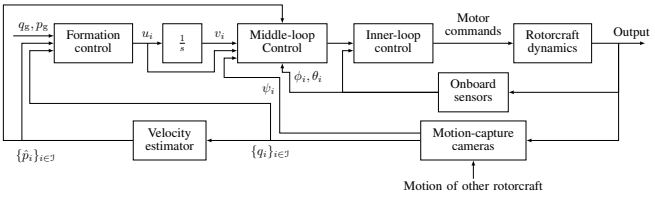

Fig. 10. The ith quadcopter computes the outer-loop formation control u_i from (5) using feedback $\{q_j - q_i\}_{j\in\mathcal{N}_i}$ and $\{p_j - p_i\}_{j\in\mathcal{N}_i}$ in combination with leader information (if applicable). Then, u_i and its integral v_i are sent to the middle-loop controller. The motion-capture system provides estimates of position $\{q_j\}_{j\in\mathcal{I}}$, velocity $\{p_j\}_{j\in\mathcal{I}}$, and yaw ψ_i, which are transmitted to each quadcopter over the wireless mesh network. The ith quadcopter's onboard sensors provide estimates of pitch θ_i and roll ϕ_i, which are used by the middle-loop controller.

A middle-loop velocity controller is implemented on the Pi to generate the PWM pitch, roll, and throttle commands. This middle-loop controller uses desired acceleration u_i and velocity v_i commands, and feedback of the quadcopter's yaw, pitch, roll, and velocity to determine the desired pitch, roll, and thrust. These desired commands are then converted to pitch, roll, and throttle PWM commands, which are sent to the Pixhawk's inner-loop controller via dronekit.

The dynamics of each middle-and-inner-loop stabilized quadcopter is approximated by (1) and (2), where u_i is generated by the outer-loop formation controller (5), which uses motion-capture feedback $\{q_j - q_i\}_{j\in\mathcal{N}_i}$ and $\{p_j - p_i\}_{j\in\mathcal{N}_i}$. Then, u_i is numerically integrated to obtain the desired velocity v_i, and both u_i and v_i are sent to the middle-loop controller. The block diagram in Figure 10 shows the control architecture.

We now present the results from experiments using $n = 3$ quadcopters, where (5) is implemented in the decentralized multi-loop control architecture describe above with a virtual leader. We use a separate control in the vertical direction for equipment and operator safety, which implies that $m = 2$.

Let $\mathcal{N}_1 = \{2, 3\}$, $\mathcal{N}_2 = \{1, 3\}$, and $\mathcal{N}_3 = \{1, 2\}$, which represents an undirected cyclic feedback structure. The function ϕ is given by Example 3 with $\nu = 0.25$, which yields *a priori* bounded controls and the gains are selected to prevent actuator saturation. Similar results can be obtained with ϕ given by Example 4. For all $j \in \mathcal{N}_i$, let $\alpha_{ij} = 0.15$ and $\beta_{ij} = 0.86$. Let $a_1 = 0.3$, $b_1 = 1.2$, $a_2 = a_3 = 0$, and $b_2 = b_3 = 0$. Thus, only the first agent has a measurement of its position and velocity relative to the leader.

Let $R(t) \in \mathrm{SO}(2)$ satisfy $\dot{R}(t) = R(t)\Omega$, where $R(0) = I_2$ and $\Omega = \left[\begin{smallmatrix} 0 & -0.1 \\ 0.1 & 0 \end{smallmatrix}\right]$ rad/s. Define $d_1 \triangleq [0.8 \quad 0.43]^{\mathrm{T}}$ m, $d_2 \triangleq [-0.8 \quad 0.43]^{\mathrm{T}}$ m, and $d_3 \triangleq [0 \quad -0.9]^{\mathrm{T}}$ m, which are the desired agent positions relative to the leader resolved in a frame defined by R^{T}. The desired positions are $\delta_i = Rd_i$.

Experiment 1. The leader's position is $q_g(t) \equiv [-1 \quad 0]^{\mathrm{T}}$ m, which is non-translating. Figure 11 shows that the agents approach their desired time-varying positions relative to the leader. We examine the last 30 s of data to analyze the steady-state errors. The time-and-agent-average position error is $[-11 \quad -27]^{\mathrm{T}}$ mm with a standard deviation of $[162 \quad 118]^{\mathrm{T}}$ mm. The time-and-agent-average velocity error is $[9 \quad -12]^{\mathrm{T}}$ mm/s with a standard deviation of $[107 \quad 81]^{\mathrm{T}}$ mm/s. The standard deviation in the position

error can be explained, in part, by the ground-effect airflow created by each of the quadcopters' propellers. The indoor flight facility's 3.3 m vertical limit prevents the aircraft from flying high enough to eliminate ground effect. Additionally, inaccuracies in the thrust-to-throttle mapping contribute to the standard deviation in the position error. △

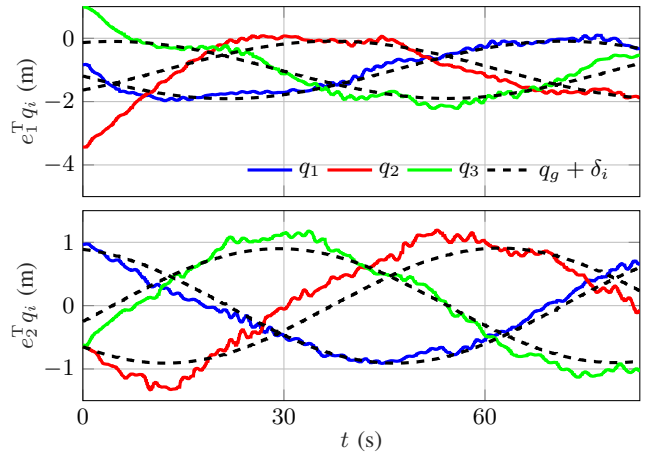

Fig. 11. Position q_i and desired position $q_{\mathrm{g}} + \delta_i$ with a non-translating leader and a time-varying formation.

Experiment 2. The leader's position is $q_{\mathrm{g}}(t) = [-1 + \sin 0.12t \quad 0]^{\mathrm{T}}$ m. Figure 12 shows that the agents approach their desired time-varying positions relative to the leader. We examine the last 30 s of data to analyze the steady-state errors. The time-and-agent-average position error is $[39 \quad -13]^{\mathrm{T}}$ mm with a standard deviation of $[188 \quad 141]^{\mathrm{T}}$ mm. The time-and-agent-average velocity error is $[-6 \quad 6]^{\mathrm{T}}$ mm/s with a standard deviation of $[95 \quad 84]^{\mathrm{T}}$ mm/s. These steady-state errors are comparable to those in Experiment 1. △

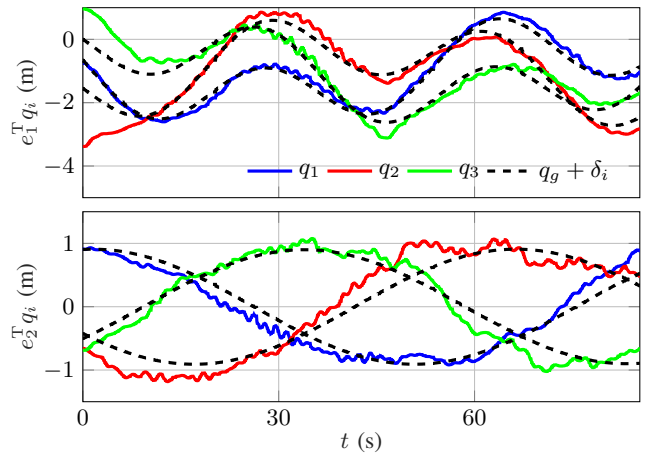

Fig. 12. Position q_i and desired position $q_{\mathrm{g}} + \delta_i$ with a translating leader and a time-varying formation.

IX. Outdoor Rotorcraft Experiments

This section presents results from outdoor experiments using three 3D-Robotics Solo quadcopters. These outdoor

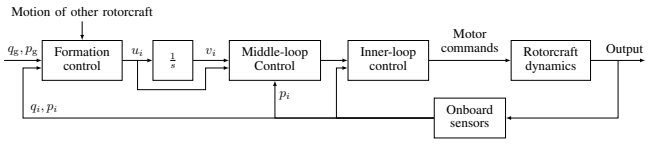

Fig. 13. The ith quadcopter computes the outer-loop formation control u_i from (5) using feedback $\{q_j - q_i\}_{j \in \mathcal{N}_i}$ and $\{p_j - p_i\}_{j \in \mathcal{N}_i}$ in combination with leader information (if applicable). Then, u_i and its integral v_i are sent to the middle-loop controller. The feedback q_i and p_i are obtained from onboard GPS, whereas wireless mesh communication is used to obtain $\{q_j\}_{j \in \mathcal{N}_i}$ and $\{p_j\}_{j \in \mathcal{N}_i}$ and the leader information (if applicable).

experiments demonstrate the formation control algorithm in a real-world environment with exogenous disturbances (e.g., wind) and with only onboard sensing (e.g., GPS and IMU) in place of an off-board motion capture system.

Each quadcopter uses onboard GPS and IMUs to obtain estimates of its inertial position and velocity. This feedback data is transmitted to other aircraft at 10 Hz using an ad hoc wireless mesh network. Each quadcopter is attitude stabilized using the Arducopter 3.3 inner-loop controller in 'guided' mode, which is implemented on the quadcopter's onboard Pixhawk Cube 2.0 flight controller. The inner-loop controller accepts velocity commands over micro air vehicle (MAV) link using the dronekit API.

The velocity commands are sent to the Pixhawk's inner-loop controller from the onboard Raspberry Pi 3B+ at 10 Hz through the serial2 port in the quadcopter's accessory bay (see Figure 9). The Pi obtains feedback measurements of the quadcopter's position and velocity from the Pixhawk's onboard sensors and an extended-Kalman filter.

A middle-loop velocity controller is implemented on the Pi to generate the velocity commands. This middle-loop controller uses desired acceleration u_i and desired velocity v_i commands, and feedback of the quadcopter's velocity to determine a commanded velocity, which is sent to the Pixhawk's inner-loop controller over MAV link using dronekit.

The dynamics of each middle-and-inner-loop stabilized quadcopter is approximated by (1) and (2), where u_i is generated by the outer-loop formation controller (5), which uses feedback of $\{q_j - q_i\}_{j \in \mathcal{N}_i}$ and $\{p_j - p_i\}_{j \in \mathcal{N}_i}$ obtained from each vehicle's onboard sensors and intervehicle communication over the ad hoc wireless mesh network. Then, u_i is numerically integrated to obtain the desired velocity v_i, and both u_i and v_i are sent to the middle-loop controller. In addition, a ground-station computer generates the virtual leader information in a north-east-down reference frame, and if applicable, transmits this data to the quadcopters. The block diagram in Figure 13 shows the control architecture.

We now present the results from experiments using $n = 3$ quadcopters, where (5) is implemented in the decentralized multi-loop control architecture described above with $m = 3$. These experiments were conducted at the University of Kentucky Agronomy Farm located in Lexington, Kentucky, with 6–8 mph steady winds blowing from the west–northwest direction. Each flight was conducted under the Federal Aviation Administration's Part 107 guidelines.

Let $\mathcal{N}_1 = \varnothing$, $\mathcal{N}_2 = \{1\}$, and $\mathcal{N}_3 = \{1\}$. The function ϕ

is given by Example 3 with $\nu = 0.25$, which implies that $\phi_0 = 1$. For all $j \in \mathcal{N}_i$, let $\alpha_{ij} = 0.2$, and let $a_1 = 0.3$ and $a_2 = a_3 = 0$. Let $\kappa = 4.33$, which satisfies (24) because $\sqrt{2\lambda_{\max}(D^{1/2}Q^{-1}D^{1/2})} = 2.69$. Thus, we let $\beta_{ij} = \kappa\alpha_{ij} = 0.866$, $b_1 = \kappa a_i = 1.3$, and $b_2 = b_3 = 0$, which implies that only the first agent has a measurement of it position and velocity relative to the leader.

Let $R(t) \in \mathrm{SO}(3)$ satisfy $\dot{R}(t) = R(t)\Omega$, where $R(0) = I_3$, where $\Omega \in \mathrm{so}(3)$ is specified in each experiment. Define $d_1 \triangleq [3 \quad 2 \quad 0]^{\mathrm{T}}$ m, $d_2 \triangleq [-3 \quad 2 \quad -3]^{\mathrm{T}}$ m, and $d_3 \triangleq [0 \quad -3 \quad -1.5]^{\mathrm{T}}$ m, which are the desired agent positions relative to the leader resolved in a frame defined by R^{T}. Thus, the desired time-varying positions are $\delta_i = Rd_i$. The leader's position is $q_{\mathrm{g}}(t) = \left[\begin{array}{ccc} 4\cos\frac{\pi t}{15} & -4\sin\frac{\pi t}{15} & -10 + 2\sin\frac{\pi t}{15} \end{array}\right]^{\mathrm{T}}$ m

Experiment 3. The angular velocity is $\Omega = 0.3[e_3]_\times$ rad/s. Figure 14 shows the three-dimensional agent trajectories q_i and the desired trajectories $q_{\mathrm{g}} + \delta_i$ from $t_1 = 15$ s to $t_2 = 30$ s. By $t_2 = 30$ s, the agents reach and maintain the desired time-varying formation. Figure 15 and Figure 16 show that the agents approach their desired positions and velocities. We examine the last 30 s of data to analyze the steady-state errors. The time-and-agent-average position error is $[15 \quad 2 \quad -18]^{\mathrm{T}}$ mm with a standard deviation of $[173 \quad 172 \quad 191]^{\mathrm{T}}$ mm. The time-and-agent-average velocity error is $[-4 \quad -6 \quad 7]^{\mathrm{T}}$ mm/s with a standard deviation of $[149 \quad 151 \quad 78]^{\mathrm{T}}$ mm/s. The standard deviation in the position and velocity error can be explained, in part, by the wind as well as time delay from communication latency. △

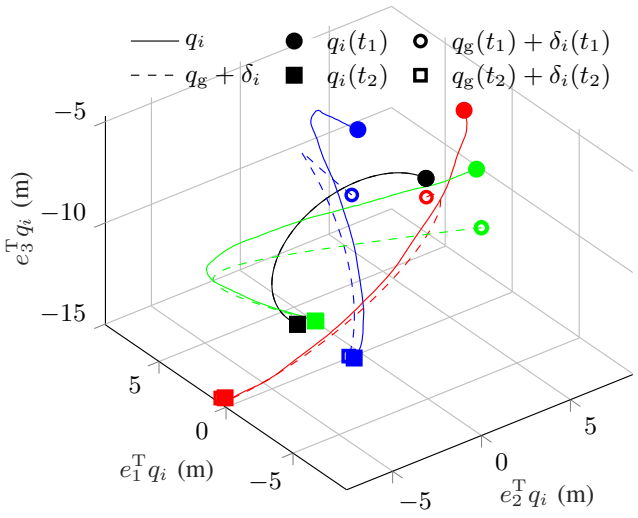

Fig. 14. Three-dimensional agent position q_i and desired time-varying position $q_{\mathrm{g}} + \delta_i$ from $t_1 = 15$ s to $t_2 = 30$ s for agents $i = 1$ (blue), $i = 2$ (red), and $i = 3$ (green). The leader trajectory q_{g} is shown in black. By $t_2 = 30$ s, the agents achieve and maintain the desired time-varying formation.

Experiment 4. The angular velocity is $\Omega = -0.15[e_1]_\times$ rad/s. Figure 17 shows the three-dimensional agent trajectories q_i and the desired trajectories $q_{\mathrm{g}} + \delta_i$ from $t_1 = 15$ s to $t_2 = 30$ s. By $t_2 = 30$ s, the agents reach and maintain the desired time-varying formation. Figure 18 and Figure 19 show that the agents approach their desired positions and

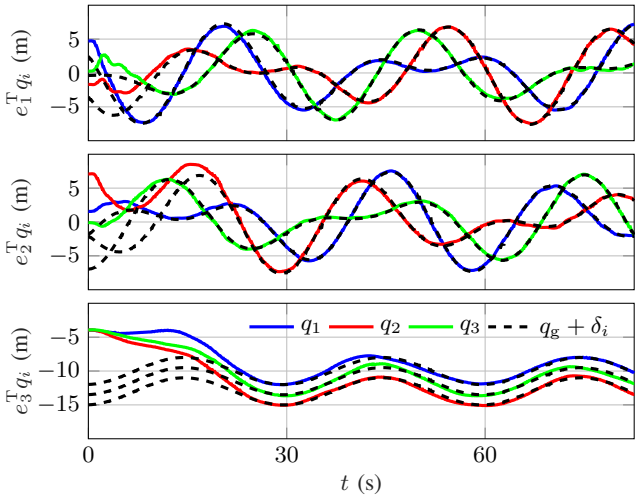

Fig. 15. Position q_i and desired position $q_{\mathrm{g}} + \delta_i$ with a translating leader and a time-varying formation.

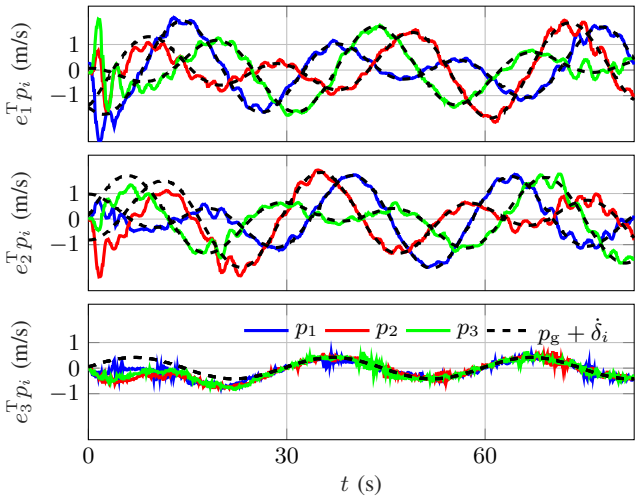

Fig. 16. Velocity p_i and desired velocity $p_{\mathrm{g}} + \dot{\delta}_i$ with a translating leader and a time-varying formation.

velocities. We examine the last 30 s of data to analyze the steady-state errors. The time-and-agent-average position error is $[-19 \quad -33 \quad -69]^{\mathrm{T}}$ mm with a standard deviation of $[111 \quad 133 \quad 240]^{\mathrm{T}}$ mm. The time-and-agent-average velocity error is $[-1 \quad 8 \quad 13]^{\mathrm{T}}$ mm/s with a standard deviation of $[114 \quad 92 \quad 70]^{\mathrm{T}}$ mm/s. These steady-state errors are comparable to those in Experiment 3. △

X. Conclusions

This paper presented a new leader-following formation control for double-integrator dynamics, where the desired positions δ_i are potentially time varying. Notably, the method incorporates a control function ϕ, which belongs to a general class of nonlinear functions. For example, ϕ can be selected such that the agents' controls are bounded, which can account for actuator magnitude saturation. The algorithm also includes collision-avoidance terms that for a set of initial conditions, prevent each agent from colliding with the agents in its

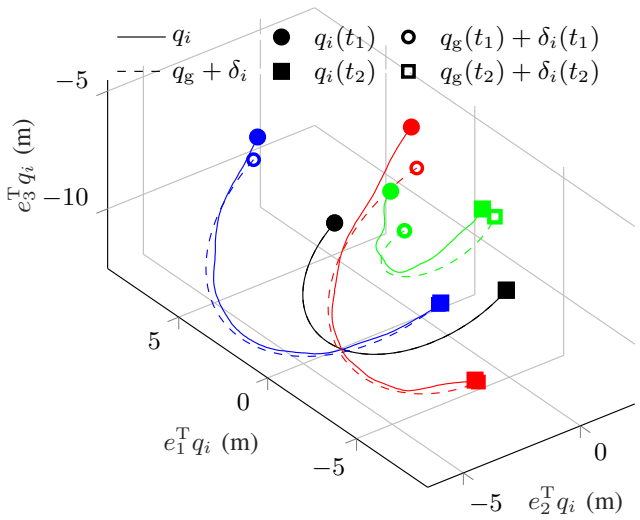

Fig. 17. Three-dimensional agent position q_i and desired time-varying position $q_{\mathrm{g}}+\delta_i$ from $t_1 = 15$ s to $t_2 = 30$ s for agents $i = 1$ (blue), $i = 2$ (red), and $i = 3$ (green). The leader trajectory q_{g} is shown in black. By $t_2 = 30$ s, the agents achieve and maintain the desired time-varying formation.

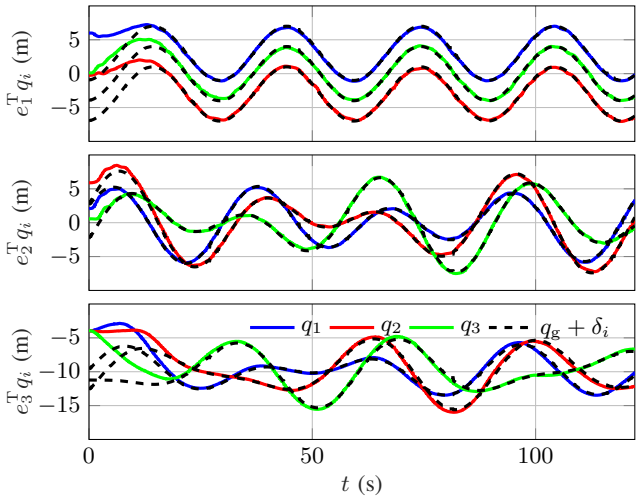

Fig. 18. Position q_i and desired position $q_{\mathrm{g}}+\delta_i$ for a translating leader and a time-varying formation.

neighbor set or with the leader (if applicable). This new algorithm was analyzed with both undirected and directed communication. Finally, we demonstrated the method in numerical examples as well as indoor and outdoor rotorcraft experiments. This paper's time-varying formation approach has application in distributed sensing and imaging, where the target to be sensed or imaged is translating and rotating.

Appendix A
Proof of Lemmas 1, 2, and 4

Proof of Lemma 1: Note that

$$\sum_{(i,j)\in\mathcal{P}} a_{ij}x_i^{\mathrm{T}}\phi(y_j-y_i) = \frac{1}{2}\sum_{(i,j)\in\mathcal{P}}\big[a_{ij}x_i^{\mathrm{T}}\phi(y_j-y_i) + a_{ji}x_j^{\mathrm{T}}\phi(y_i-y_j)\big].$$

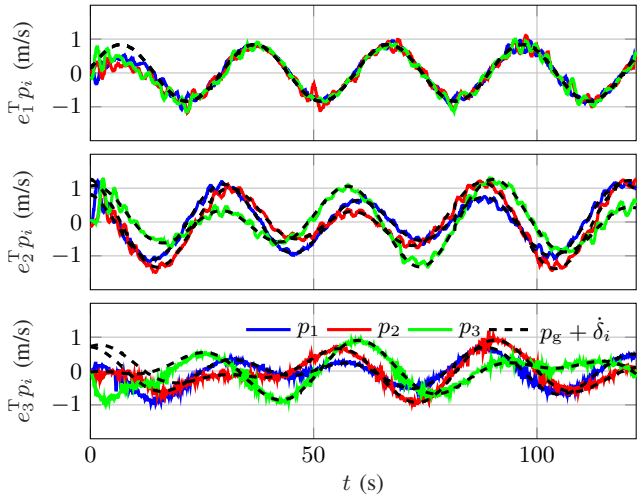

Fig. 19. Velocity p_i and desired velocity $p_{\mathrm{g}}+\dot{\delta}_i$ for a translating leader and a time-varying formation.

Then, using (C2) and $a_{ij} = a_{ji}$ yields the result. ■

Proof of Lemma 2: Since $\mathcal{A}$ is a Laplacian and $\mathcal{A}_{\mathrm{d}}$ is positive semidefinite and diagonal, it follows that $N \triangleq \mathcal{A}+\mathcal{A}_{\mathrm{d}}$ is diagonally dominant. Let $v_l \in \mathcal{I}\backslash\{\ell\}$. Since ℓ is a center vertex of the quasi-strongly connected graph $\mathcal{G}$, it follows that $\mathcal{G}$ has a walk of length l from ℓ to v_l. Thus, there exists an $(l+1)$-tuple $(\ell, v_1, \ldots, v_l)$ such that $N_{(\ell,v_1)}, N_{(v_1,v_2)}, \ldots, N_{(v_{l-1},v_l)}$ are nonzero. Furthermore, since $\mathcal{A}$ is a Laplacian, $\mathcal{A}_{\mathrm{d}}$ is diagonal, and $a_\ell > 0$, it follows that $\sum_{j\in\mathcal{I}\backslash\{\ell\}}|N_{(\ell,j)}| = \sum_{j\in\mathcal{I}\backslash\{\ell\}}|\mathcal{A}_{(\ell,j)}| = |\mathcal{A}_{(\ell,\ell)}| < a_\ell + |\mathcal{A}_{(\ell,\ell)}| = |N_{(\ell,\ell)}|$. Thus, [52, Theorem on pp. 63] implies that N is nonsingular. ■

Proof of Lemma 4: To prove (36), we consider two cases: $\|x+\delta_i\| > d$, and $\|x+\delta_i\| \le d$. First, let $x \in \mathbb{R}^m \setminus \{0\}$ be such that $\|x+\delta_i\| > d$. In this case, (27)–(31) imply that $\sigma(x+\delta_i) = 0$, which together with (C3) confirms (36).

Next, let $x \in \mathbb{R}^m \setminus \{0\}$ be such that $\|x+\delta_i\| \le d$. In this case, (27)–(29) imply that $\psi(\|x+\delta_i\|^2) \le 0$, which combined with (31) implies that $x^{\mathrm{T}}\sigma(x+\delta_i) \le 0$. Note that $c_i > 0$ and $x^{\mathrm{T}}\phi(x) > 0$. Thus, (34) implies that $x^{\mathrm{T}}\phi(x) + \frac{1}{c_i}x^{\mathrm{T}}\sigma(x+\delta_i) \ge 0$, which, combined with $x^{\mathrm{T}}\sigma(x+\delta_i) \le 0$ and $\varepsilon_i \in [0,1)$, confirms (36).

Finally, note that the same arguments show (37). ■

References

[1] T. Bonin, P. Chilson, B. Zielke, and E. Federovich, "Observations of the early evening boundary-layer transition using a small unmanned aerial system," *Boundary-Layer Meteorol.*, vol. 146, pp. 119–132, 2013.

[2] R. W. Beard, T. W. McLain, D. B. Nelson, D. Keingston, and D. Johnson, "Decentralized cooperative aerial surveillance using decentralized cooperative aerial surveillance using fixed-wing miniature UAVs," *Proc. IEEE*, vol. 94, no. 7, pp. 1306–1324, 2006.

[3] J. Ota, "Multi-agent robot systems as distributed autonomous systems," *Adv. Eng. Informat.*, vol. 20, no. 1, pp. 59–70, 2006.

[4] Y. Cao, W. Yu, W. Ren, and G. Chen, "An overview of recent progress in the study of distributed multi-agent coordination," *IEEE Trans. Industrial Informatics*, vol. 9, pp. 427–438, Feb 2013.

[5] R. Olfati-Saber, J. A. Fax, and R. M. Murray, "Consensus and cooperation in networked multi-agent systems," *Proc. IEEE*, vol. 95, pp. 215–233, 2007.

[6] W. Ren, R. W. Beard, and E. M. Atkins, "Information consensus in multivehicle cooperative control," *IEEE Contr. Sys. Mag.*, vol. 27, no. 2, pp. 71–82, 2007.

[7] W. Ren, "Consensus strategies for cooperative control of vehicle formations," *IET Contr. Theory App.*, vol. 1, pp. 505–512, 2007.

[8] J. Qin and H. Gao, "A sufficient condition for convergence of sampled-data consensus for double-integrator dynamics with nonuniform and time-varying communication delays," *IEEE Trans. Autom. Contr.*, vol. 57, no. 9, pp. 2417–2422, 2012.

[9] W. Yu, W. X. Zheng, G. Chen, W. Ren, and J. Cao, "Second-order consensus in multi-agent dynamical systems with sampled position data," *Automatica*, vol. 47, no. 7, pp. 1496–1503, 2011.

[10] J. Zhu, Y.-P. Tian, and J. Kuang, "On the general consensus protocol of multi-agent systems with double-integrator dynamics," *Lin. Alg. its App.*, vol. 431, no. 5, pp. 701 – 715, 2009.

[11] P. Lin and Y. Jia, "Consensus of second-order discrete-time multi-agent systems with nonuniform time-delays and dynamically changing topologies," *Automatica*, vol. 45, no. 9, pp. 2154–2158, 2009.

[12] F. Chen, Z. Chen, L. Xiang, Z. Liu, and Z. Yuan, "Reaching a consensus via pinning control," *Automatica*, vol. 45, pp. 1215 – 1220, 2009.

[13] Y. Cao, D. Stuart, W. Ren, and Z. Meng, "Distributed containment control for multiple autonomous vehicles with double-integrator dynamics: Algorithms and experiments," *IEEE Trans. Contr. Sys. Tech.*, vol. 19, pp. 929–938, July 2011.

[14] Y. Hong, J. Hu, and L. Gao, "Tracking control for multi-agent consensus with an active leader and variable topology," *Automatica*, vol. 42, no. 7, pp. 1177 – 1182, 2006.

[15] Y. Cao and W. Ren, "Distributed coordinated tracking with reduced interaction via a variable structure approach," *IEEE Trans. Autom. Contr.*, vol. 57, no. 1, pp. 33–48, 2012.

[16] Y. Zhang and Y. P. Tian, "Consensus of data-sampled multi-agent systems with random communication delay and packet loss," *IEEE Trans. Autom. Contr.*, vol. 55, pp. 939–943, April 2010.

[17] Y. Gao and L. Wang, "Sampled-data based consensus of continuous-time multi-agent systems with time-varying topology," *IEEE Trans. Autom. Contr.*, vol. 56, no. 5, pp. 1226–1231, 2011.

[18] Z. Li, G. Wen, Z. Duan, and W. Ren, "Designing fully distributed consensus protocols for linear multi-agent systems with directed graphs," *IEEE Trans. on Autom. Contr.*, vol. 60, no. 4, pp. 1152–1157, 2015.

[19] G. Lafferriere, A. Williams, J. Caughman, and J. J. P. Veerman, "Decentralized control of vehicle formations," *Syst. Contr. Lett.*, vol. 54, no. 9, pp. 899–910, 2005.

[20] W. Ni and D. Cheng, "Leader-following consensus of multi-agent systems under fixed and switching topologies," *Syst. Contr. Lett.*, vol. 59, no. 3–4, pp. 209–217, 2010.

[21] C. Tan and G. Liu, "Consensus of discrete-time linear networked multi-agent systems with communication delays," *IEEE Trans. Autom. Contr.*, vol. 58, no. 11, pp. 2962–2968, 2013.

[22] G. Gu, L. Marinovici, and F. L. Lewis, "Consensusability of discrete-time dynamic multiagent systems," *IEEE Trans. Autom. Contr.*, vol. 57, no. 8, pp. 2085–2089, 2012.

[23] C. Heintz and J. B. Hoagg, "Formation control for agents modeled with extended unicycle dynamics that includes orientation kinematics on SO(m) and speed constraints," *Sys. Contr. Lett.*, vol. 146, pp. 104784:1–13, 2020.

[24] W. Yu, G. Chen, M. Cao, and J. Kurths, "Second-order consensus for multiagent systems with directed topologies and nonlinear dynamics," *IEEE Trans. Sys., Man, and Cyb., Part B*, vol. 40, pp. 881–891, 2010.

[25] Q. Song, J. Cao, and W. Yu, "Second-order leader-following consensus of nonlinear multi-agent systems via pinning control," *Sys. Contr. Lett.*, vol. 59, no. 9, pp. 553 – 562, 2010.

[26] D. M. Stipanović, G. Inalhan, R. Teo, and C. J. Tomlin, "Decentralized overlapping control of a formation of unmanned aerial vehicles," *Automatica*, vol. 40, no. 8, pp. 1285–1296, 2004.

[27] L. Moreau, "Stability of multiagent systems with time-dependent communication links," *IEEE Trans. Autom. Contr.*, vol. 50, no. 2, pp. 169–182, 2005.

[28] G. Wen, Z. Duan, W. Yu, and G. Chen, "Consensus of multi-agent systems with nonlinear dynamics and sampled-data information: a delayed-input approach," *Int. J. Robust Nonl. Contr.*, vol. 23, pp. 602–619, 2013.

[29] R. A. Chavan, S. Wang, T. M. Seigler, and J. B. Hoagg, "Consensus on so(3) with piecewise-continuous sinusoids," *Automatica*, vol. 122, p. 109262, 2020.

[30] W. Song, J. Thunberg, X. Hu, and Y. Hong, "Distributed high-gain attitude synchronization using rotation vectors," *Journal of Systems Science and Complexity*, vol. 28, pp. 289–304, Apr 2015.

[31] J. Thunberg, W. Song, E. Montijano, Y. Hong, and X. Hu, "Distributed attitude synchronization control of multi-agent systems with switching topologies," *Automatica*, vol. 50, no. 3, pp. 832–840, 2014.

[32] J. R. Lawton and R. W. Beard, "Synchronized multiple spacecraft rotations," *Automatica*, vol. 38, no. 8, pp. 1359–1364, 2002.

[33] D. V. Dimarogonas, P. Tsiotras, and K. J. Kyriakopoulos, "Leader–follower cooperative attitude control of multiple rigid bodies," *Sys. Contr. Lett.*, vol. 58, no. 6, pp. 429–435, 2009.

[34] A. Sarlette, R. Sepulchre, and N. E. Leonard, "Autonomous rigid body attitude synchronization," *Automatica*, vol. 45, pp. 572–577, 2009.

[35] Y. Cao and W. Ren, "Multi-vehicle coordination for double-integrator dynamics under fixed undirected/directed interaction in a sampled-data setting," *Int. J. Robust Nonlinear Contr.*, vol. 20, pp. 987–1000, 2010.

[36] S. Martin, A. Girard, A. Fazeli, and A. Jadbabaie, "Multiagent flocking under general communication rule," *IEEE Trans. Contr. Networked Syst.*, vol. 1, no. 2, pp. 155–166, 2014.

[37] X. Dong, B. Yu, Z. Shi, and Y. Zhong, "Time-varying formation control for unmanned aerial vehicles: Theories and applications," *IEEE Trans. on Contr. Sys. Tech.*, vol. 23, no. 1, pp. 340–348, 2015.

[38] R. Wang, X. Dong, Q. Li, and Z. Ren, "Distributed adaptive formation control for linear swarm systems with time-varying formation and switching topologies," *IEEE access : practical innovations, open solutions.*, vol. 4, pp. 8995–9004, 2016.

[39] X. Dong and G. Hu, "Time-varying formation tracking for linear multiagent systems with multiple leaders," *IEEE transactions on automatic control*, vol. 62, no. 7, pp. 3658–3664, 2017.

[40] D. Zhang and G. Duan, "Leader-following fixed-time output feedback consensus for second-order multi-agent systems with input saturation," *Int. J. of Sys. Sci.*, vol. 49, no. 14, pp. 2873–2887, 2018.

[41] Z. Zhao and Z. Lin, "Global leader-following consensus of a group of general linear systems using bounded controls," *Automatica*, vol. 68, pp. 294 – 304, 2016.

[42] X. Lu, S. Chen, and J. L, "Finite-time tracking for double-integrator multi-agent systems with bounded control input," *IET Contr. Theory App.*, vol. 7, pp. 1562–1573(11), July 2013.

[43] B. Zhu, C. Meng, and G. Hu, "Robust consensus tracking of doubleintegrator dynamics by bounded distributed control," *Int. J. of Robust Nonl. Contr.*, vol. 26, no. 7, pp. 1489–1511, 2016.

[44] W. Ren, "On consensus algorithms for double-integrator dynamics," *IEEE Trans. Autom. Contr.*, vol. 53, no. 6, pp. 1503–1509, 2008.

[45] B. J. Wellman and J. B. Hoagg, "A flocking algorithm with individual agent destinations and without a centralized leader," *Sys. Contr. Lett.*, vol. 102, pp. 57–67, 2017.

[46] R. Olfati-Saber, "Flocking for multi-agent dynamic systems: Algorithms and theory," *IEEE Trans. Autom. Contr.*, vol. 51, pp. 401–420, 2006.

[47] J. Zhou, Y. Guo, G. Li, and J. Zhang, "Event-triggered control for nonlinear uncertain second-order multi-agent formation with collision avoidance," *IEEE Access*, vol. 7, pp. 104489–104499, 2019.

[48] A. Mondal, C. Bhowmick, L. Behera, and M. Jamshidi, "Trajectory tracking by multiple agents in formation with collision avoidance and connectivity assurance," *IEEE Systems J.*, vol. 12, pp. 2449–2460, 2018.

[49] H. K. Khalil, *Nonlinear Systems*. Prentice Hall, 3rd ed., 1996.

[50] H. Zhang and F. L. Lewis, "Adaptive cooperative tracking control of higher-order nonlinear systems with unknown dynamics," *Automatica*, vol. 48, no. 7, pp. 1432 – 1439, 2012.

[51] D. S. Bernstein, *Matrix Mathematics*. Princeton University Press, second ed., 2009.

[52] P. Shivakumar and K. H. Chew, "A sufficient condition for nonvanishing of determinants," *Proceedings of the American mathematical society*, pp. 63–66, 1974.

Zachary S. Lippay received the B.S. degree in Mechanical Engineering from the University of Kentucky in 2016. He is currently a Ph.D. candidate in the department of Mechanical Engineering at the University of Kentucky.

Jesse B. Hoagg received the B.S.E. degree in Civil and Environmental Engineering from Duke University in 2002, the M.S.E. degree in Aerospace Engineering from the University of Michigan in 2003, the M.S. degree in Mathematics from the University of Michigan in 2005, and the Ph.D. degree in Aerospace Engineering from the University of Michigan in 2006. He is currently the Donald and Gertrude Lester Professor of Mechanical Engineering at the University of Kentucky.